Environmental Science and Pollution Research (2024) 31:51267–51299
https://doi.org/10.1007/s11356-024-34493-2

RESEARCH ARTICLE

Effective degradation of bentazone by two-dimensional and three-phase, three-dimensional electro-oxidation system: kinetic studies and optimization using ANN

Canan Samdan[1] · Hakan Demiral[1] · Yunus Emre Simsek[2] · Ilknur Demiral[1] · Belgin Karabacakoglu[1] · Tugce Bozkurt[3] · Hatice Hurrem Cin[3]

Received: 22 April 2024 / Accepted: 22 July 2024 / Published online: 6 August 2024
© The Author(s), under exclusive licence to Springer-Verlag GmbH Germany, part of Springer Nature 2024

Abstract

Bentazone is a broad-leaved weed-specific herbicide in the pesticide industry. This study focused on removing bentazone from water using three different methods: a two and three-dimensional electro-oxidation process (2D/EOP and 3D/EOP) with a fluid-type reactor arrangement using tetraethylenepentamine-loaded particle electrodes and an adsorption method. Additionally, we analysed the effects of two types of supporting electrolytes (Na_2SO_4 and NaCl) on the degradation process. The energy consumption amounts were calculated to evaluate the obtained results. The degradation reaction occurs 3.5 times faster in 3D/EOP than in 2D/EOP at 6 V in Na_2SO_4. Similarly, the degradation reaction of bentazone in NaCl occurs 2.5 times faster in 3D/EOP than in 2D/EOP at a value of 7.2 mA/cm^2. Removal of bentazone is significantly better in 3D/EOPs than in 2D/EOPs. The use of particle electrodes can significantly enhance the degradation efficiency. The study further assessed the prediction abilities of the machine learning model (ANN). The ANN presented reasonable accuracy in bentazone degradation with high R^2 values of 0.97953, 0.98561, 0.98563, and 0.99649 for 2D with Na_2SO_4, 2D with NaCl, 3D with Na_2SO_4, and 3D with NaCl, respectively.

Keywords TEPA · Loaded particle electrodes · Three phase, three dimensional · Electro oxidation reactor · Bentazone degradation · Artificial neural network (ANN)

Introduction

Pesticides represent a category of synthetic organic compounds that are systematically utilized to mitigate and control undesirable organisms, particularly within agricultural landscapes. Water supplies containing pesticides have a negative impact on humans and ecosystems. These materials are considered possible mutagens because they contain components that trigger deviations in DNA. Around 2.7 million tons of pesticides were used worldwide in 2020, according

Responsible Editor: Guilherme Luiz Dotto

✉ Canan Samdan
caydin@ogu.edu.tr

Hakan Demiral
hdemiral@ogu.edu.tr

Yunus Emre Simsek
yunusemre.simsek@bilecik.edu.tr

Ilknur Demiral
idemiral@ogu.edu.tr

Belgin Karabacakoglu
bkara@ogu.edu.tr

Tugce Bozkurt
tugceb.9519@gmail.com

Hatice Hurrem Cin
cinhurremhatice@gmail.com

[1] Department of Chemical Engineering, Faculty of Engineering and Architecture, Eskisehir Osmangazi University, 26480 Eskişehir, Turkey

[2] Department of Chemical Engineering, Faculty of Engineering, Bilecik Şeyh Edebali University, 11100, TR, Bilecik, Turkey

[3] Chemical Engineering Department, Eskişehir Osmangazi University, 26480 Eskişehir, Turkey

to FAO (FAO 2022). Turkey is ranked 12th in the world, behind the USA (407779 t), Brazil (377176 t), and China (273375 t). When pesticides are applied to soil, water, air, and agricultural areas, other creatures living in these environments also come into contact with pesticides (FAOSTAT 2023). The environments where pesticides are applied are affected by their chemical structure, physical properties, formulation type, application method, climate, and agricultural conditions. Numerous studies on the design of selective, easy-to-operate, easy-to-install treatment processes for the intelligent disposal of pesticides reaching water for various reasons are attracting worldwide attention.

Bentazone is a synthetic compound belonging to the thiadiazole chemical class (Gaynor and MacTavish 1981). The assessment of bentazone was conducted by the Joint Food and Agriculture Organization of the United Nations (FAO)/World Health Organization (WHO) Meeting on Pesticide Residues (JMPR) in 2016 (FAO/WHO 2016). Ingestion of bentazone can lead to symptoms such as fevers, kidney failure, tachycardia, dyspnoea, and hyperthermia. It is rapidly metabolized by pesticide-resistant plants and animals (FAO/WHO 2016). However, it should be noted that adequate examination has not been carried out on humans. Its high-water solubility and low soil adsorption may lead to leaching during heavy rainfall, making it a concern for water pollution. Bentazone is commonly detected in European ground and surface waters, so monitoring its presence is crucial due to its wide use as a herbicide (Cerejeira et al. 2003; Ricart et al. 2010).

Electro-oxidation systems offer several advantages over conventional purification methods for the degradation of bentazone. However, these also have some limitations. The advantages are as follows.

Electro-oxidation systems can achieve high degradation efficiency without creating harmful residues, and these systems are environmentally friendly (Li et al. 2019). The inclusion of microparticle particles increases the surface area for adsorbing and catalytically oxidizing contaminants (Ji et al. 2018b; Yu et al. 2020). Electro-oxidation systems can be easily optimized by adjusting parameters such as current density, electrolyte concentration, and applied voltage (Liu et al. 2019; Ouarda et al. 2020; Cai et al. 2023). They also require fewer chemical additives, leading to reduced chemical consumption and reduced chemical processing risks (Panizza and Cerisola 2003; Ouarda et al. 2020). Electro-oxidation systems can be easily automated and controlled, allowing for more efficient and continuous operation, especially in large-scale treatment plants (Pavithra et al. 2020). Electrochemical technology has disadvantages such as high voltage and energy consumption (Deng et al. 2020).

The 2D/EOP electro-oxidation process occurs between the anode and cathode electrodes in an ionized solution in the electrolytic cell. This process has the potential to oxidize both organic and inorganic compounds (Zhou and Lei 2006; Carvalho et al. 2023). Oxidation reactions change organic materials into CO_2, H_2O, and other inorganic compounds at the anode. At the cathode, oxygen gas is formed by reduction reactions (Ghorbani et al. 2020).

Advanced treatment methods include the combined examination of adsorption and catalytic biodegradation (Han et al. 2023) and photocatalytic and biodesulfurization methods (Ahmad et al. 2023). However, in a traditional two-dimensional electrochemical reactor, the contact area cannot be increased (Kumar et al. 2014). Since the catalytic reactivity of the electrochemical system can be improved using microelectrodes, electrochemical technologies based on a fluidized bed containing particles that can move continuously, especially in cleaning various waters, have attracted great interest. The 3D electro-oxidation process (3D/EOP) is efficient because it involves functionalized small particles that increase the surface area where the reaction takes place, resulting in a faster reaction rate (Wu et al. 2019). As a result, microparticles facilitate the degradation of pollutants through direct electron transfer or indirect radically mediated reactions (Jing et al. 2013; Ouarda et al. 2020). It also shows a different example of the application of 3D reactors in research on microaerobic bioreactors using highly porous 3D carriers (Ahmad et al. 2017). There are various examples of studies on catalytic particles in the literature. TiO_4 particles have been used to degrade phenol (Xiao et al. 2023), and particles functionalized with lead have been utilized in the hydrochlorination of pentachlorophenol (Wang et al. 2021). Sn-F co-doped titanium dioxide nanoparticles have proven effective in photocatalytic degradation (Ancy et al. 2021). Ti-Sn-Ce/biochar particles have successfully cleaned and coked wastewater with toxic substances (Zhang et al. 2020). Sun et al. have used Bi-Sn-Sb/γ-Al_2O_3 particles in the electrocatalytic process for tetracycline removing (Sun et al. 2019) and the cleaning of refractory waters, respectively. Additionally, particles made from functionalized sludge have been used to clean refractory waters (Meng et al. 2019).

Tetraethylenepentamine (TEPA, $C_8H_23N_5$) is an organic base with five amino groups within its structure. TEPA can form complexes and coordination compounds through reactions with various compounds. Materials such as carbon fibres (Roy et al. 2023), nanotubes (Khoshraftar et al. 2023), lignin (Cheng et al. 2024), resin (Samaddoost et al. 2023), silica (Ahmadian Hosseini and Jahandar Lashaki 2023), silica aerogel (Huang et al. 2023), ZIF-8 SBA-15 (Wang et al. 2024), metal–organic frameworks (Dinda 2023), and activated carbons (Zhao et al. 2023; Yang et al. 2024) can capture CO_2 when modified with TEPA-containing N atoms. TEPA is employed in constructing TEPA-loaded magnetic nanoparticles to trap phosphopeptides (Zhang et al. 2023). TEPA is also used to fabricate nanoporous silicon to selectively adsorb Hg(II) in industrial wastewater (Sun et al. 2023). Additionally, it is utilized in the creation of diverse

composites (Cao 2023), including the synthesis of nanofibre hybrid membranes (Guo et al. 2023), the modification of graphene oxide (Musielak et al. 2024), the alteration of magnetic nanocomposites (Hu et al. 2024), and the design of nanocomposites for energy storage and photocatalytic degradation applications (Akram et al. 2024).

The characteristics of electrode materials significantly influence the efficiency of bentazone degradation during electro-oxidation processes. Electrodes are usually made of materials such as platinum (Wang et al. 2014), titanium (Zheng et al. 2016; Wu et al. 2019), and graphite (Kong et al. 2010; Rostami et al. 2015). Also, other inactive metals can be used for the electro-oxidation process. The electrode material is the most important factor affecting the cost of electrochemical processes. Platinum, titanium, and palladium electrodes (Jing et al. 2013; Isarain-Chávez et al. 2017; Arjona et al. 2022) are the most commonly used types of electrode for electrochemical processes due to their high reactivity and corrosion resistance. However, because these materials are quite expensive, they can be costly, especially in large-scale industrial applications. Recent research has focused on synthesizing new materials, considering properties such as the electrode material's surface area, conductivity, stability, surface chemistry, and selectivity.

Recently, various studies have shown that carbon fibre, which has a surface area of 400 to 1000 m^2/g and low electrical resistance, can successfully remove various pollutants in electrochemical processes (Hu et al. 2015; Liu et al. 2018; Wang et al. 2019; Zhu et al. 2019). The microtextures of activated carbon fibres, directly accessible from the outer fibre surface, provide rapid intra-particle diffusion and show low resistance to mass transfer. This makes them ideal candidates for wastewater treatment. Electrochemical techniques involving carbon cloths with a high specific surface area are innovative and environmentally friendly. Since activated carbon cloths do not require special shaping, they can be used directly as electrode material (Gineys et al. 2017).

Artificial neural network (ANN) involves complicated computations and mathematics that mimic human brain processes. Similar to the structure of the human brain, the ANN models consist basically of neurons interconnected to each other in a complex form. ANN is based on the process of learning. Learning is the adaption of the ANN network to better manage a task by considering sample observations (inputs). Learning entails adjusting the weights of the network to enhance the accuracy of the observed results (outputs). ANN has been employed in a wide range of applications: computer science (Al-Laham et al. 2023), mathematics (Ghattas and Manzon 2023), physics and astronomy (Basir and Senocak 2022; Liu et al. 2024), energy and its applications (Veljkovic et al. 2023), materials science (Xiao et al. 2023), medicine and dentistry (Joudi et al. 2022; Abdulaal et al. 2024), agriculture (Talaviya et al. 2020), and environmental disciplines (Konya and Nematzadeh 2024). Significant removal and degradation of pesticides from water and wastewater systems include physical, chemical, and biological technologies (Saleh et al. 2020). The degradation efficiency of electro catalytic reactors as a chemical technology depends on different operating factors such as applied potential difference, current density particle, particle electrode types and dose, electrolyte types and concentration, and pH. ANN can be employed to predict and optimize these factors (Malla et al. 2023). Some studies have mentioned the use of ANN in different types of treatment methods, including the degradation of glyphosate by microbially assisted method (Nourouzi et al. 2012), the removal of 2,4-dichlorophenoxyacetic acid (2,4-D) by using polypyrrole-coated Fe_2O_3 nanoparticle adsorbents (Fe_2O_3@PPy) (Sridevi et al. 2023), the adsorption of metolachlor by a MIL-53(Al) metal–organic framework adsorbent (Ahmad Isiyaka et al. 2022), and the separation of different types of herbicides by Liquid Chromatography (Tran et al. 2007). No studies, to the best our knowledge, relating to herbicide by 2D and 3D electrocatalytic oxidation process have been reported in the literature.

This study examined the removal of bentazone from water by two different methods. These methods are the two-dimensional electrooxidation process (2D/EOP) and the three-dimensional electrooxidation process (3D/EOP), in which electrochemical degradation occurs using TEPA-charged particle electrodes in an electrochemical reactor with a three-phase, three-dimensional fluidized type reactor arrangement. pH, electrolyte concentration, applied voltage, and current density parameters were examined to see how they affect the degradation efficiency of bentanone in 2D/EOP and 3D/EOP. Furthermore, kinetic models were used to evaluate the results. Optimization and validation of the variables affecting these processes were determined by ANN. In addition, kinetic analysis, degradation mechanism, energy consumption, and synergistic effect were comparatively studied.

Experimental method

Materials

Commercial DARCO 12–80 mesh granular activated carbon (C/AC) was used. Nitric acid (Merck—EMPLURA®; HNO_3) was used in the pre-acid modification of C/AC. Tetraethylenepentamine (Sigma-Aldrich technical grade; TEPA ($NH_2CH_2CH_2NHCH_2CH_2)_2NH$) was used to surface functionalize pre-acid-modified D/ACs. Bentazone ($C_{10}H_{12}N_2O_3S$) was used as a sample pesticide. Some properties of bentazone are given in Table 1. NaCl (Sigma-Aldrich ACS reagent, ≥ 99.0%) and Na_2SO_4 (ACS

Table 1 Some properties of bentazone

Molecular Weight	240.28 g/mol
Chemical Formula	$C_{10}H_{12}N_2O_3S$
Group of chemicals	Thiadiazine
Group of pesticide	Herbicide
Chemical Structure Depiction	

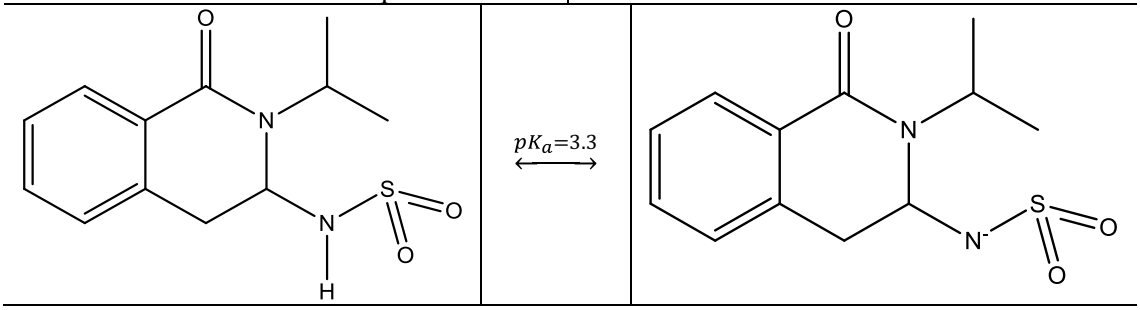

reagent, ≥ 99.0%, anhydrous powder) were used as electrolytes. The pH values of the solutions were brought to the desired value using 0.1 N HCl (Merck, ACS reagent, 37%) and 0.1 N NaOH pellets (Merck—EMPLURA®) solutions and Consort brand pH meters.

Production of particle electrodes

Acidified of C/AC for amine modification

Commercial DARCO 12–80 mesh granular activated carbon (C/AC) was used in the study. In order to purify the activated carbon from undesirable substances that may be present on its surface, a quantity of activated carbon was placed in 2 L of hot deionized water and mixed in the magnetic stirrer for 2 h. The water was filtered using strainer paper, 2 L of water was placed on it again, and the washing process continued until the water's colour became clear. C/ACs were dried in the oven at 80 °C and stored in closed containers for use in modification processes. Pre-acid modification of activated carbons using an HNO_3 solution was carried out (Tamai et al. 2006; Abd El-Magied et al. 2018; Tang et al. 2018; Azpiri Solares et al. 2019; Zhang et al. 2021). For this purpose, 15 g C/AC and 30% (v/v) HNO_3 were placed in a reaction vessel. Acidification was carried out using a magnetic stirrer for 6 h at 90 °C under a back cooler. The acidified sample was washed until the pH of the water was 5–5.5. The sample was dried in the oven at 85 °C for 24 h and used in amine modification studies.

Amine modification

Using tetraethylenepentamine (TEPA) in amine modification, the surfaces of the activated carbons are enriched with amine groups. The impact of concentration (20%, 50%, and 70% by weight) and contact time (2, 6, and 24 h) at a temperature of 80 °C on the modification of TEPA was studied. The appropriate amount of TEPA was mixed with methyl alcohol using a magnetic stick for 30 min under room conditions. The prepared solution was placed in a double-neck balloon with 5 g acidified C/AC as 1 g acidified C/AC /20 ml solution. A thermocouple is inserted into one of the necks, ensuring that the solution temperature remains constant during treatment. The modification is carried out using a magnetic stirrer at the appropriate temperature and time under the back cooler. In order to remove the TEPA molecules that are not attached to the surface in the activated carbon pores, 75 ml of ethyl alcohol was added to the activated carbons filtered by a vacuum strainer and mixed for 30 min. The samples were then washed until the pH of the water was 7. The conditions studied in amine modification and sample IDs are given in Table 2.

Determining the properties of *TEPA*/ACs

The characteristic features of the porous structures of C/AC and TEPA/ACs on which TEPA inoculated on the surface under various conditions were determined by Quantchrome Autosorb 1C device (with $N_{2(g)}$ and at 77 K). The FTIR

Table 2 Operating conditions of TEPA modification and sample codes of TEPA/ACs

Sample ID	TEPA concentration (wt%)	Time, h
20TEPA/80/6	20	6
50TEPA/80/6	50	6
70TEPA/80/6	70	6
70TEPA/80/2	70	2
70TEPA/80/24	70	24

spectra of the modified activated carbons were taken using the Fourier Transform Infrared Spectroscopy instrument. The Hitachi Regulus 8230 SEM device was used to visualize the surface pore structures. Additionally, the EDS detector connected to the SEM device was utilized to determine the samples' C, O, and N contents. Boehm titration is based on the theory that acid or base in aqueous solution reacts with various basic or acidic sites of activated carbon. The amount of oxygen-containing surface functional groups of TEPA-modified samples under various operating conditions was determined using the Boehm method. Of the sample, 0.2 g was added to 50 ml of 0.05 M $NaHCO_3$, Na_2CO_3, NaOH, and HCl solutions separately, and the surface was completely neutralized by mixing at 25 °C for 48 h. The excess base was determined using 0.1 N HCl. Total acidity was determined by titration with 0.1 N NaOH. Also, surface elemental mapping 70TEPA/80/6 was displayed using the same FE-SEM device.

A three-electrode configuration was utilized to assess the electrochemical properties of the carbon fibre electrode. The carbon fibre electrode acted as the working electrode. Platinum (1×1 cm^2) and Ag/AgCl electrodes serve as the counter and reference electrodes, respectively. Cyclic voltammetry (CV) measurements were conducted at varying scanning rates of 10, 20, 30, 40, 50, 75, and 100 mV/s within a potential window of − 3 V and + 3 V. The measurements were taken in a solution containing either 0.015 M Na_2SO_4 or 0.02 M NaCl in 100 ppm bentazone. The electrochemical measurements were performed using a Reference 3000 Potentiostat/Galvanostat/ZRA electrochemical workstation.

2D/EOP and 3D/EOP and adsorption studies

As part of our research, we utilized a three-dimensional and two-dimensional electrode system for electrochemical oxidative degradation. To set up these systems, we employed a cylindrical glass electrolytic cell measuring 5×10 mm connected to a DC power supply and constantly stirred. Both systems utilized a carbon fibre measuring 2.5×2.5 cm (6.25 cm^2) as an anode and cathode.

While the 2D/EOP electrochemical cell was constructed with a single anode and cathode, we added activated carbon produced under optimal conditions between the anode and cathode in the 3D/EOP cell, which served as particle electrodes. This allowed us to create a three-phase, three-dimensional electrochemical oxidation system within the 3D/EOP cell, which also utilized continuous mixing. Schematic view of reactors (2D/EOP and 3D/EOP) and the degradation mechanism of bentazone in 3D/EOP are shown in Fig. 14.

Before the experiments, the carbon fibre cloth was washed with deionized water. In 2D/EOP and 3D/EOP studies, bentazone concentration changes in the solution were determined for 60 min by applying different potential differences (4, 5, 6, and 7 V) to the system at an initial 100 ppm bentazone containing 0.015M Na_2SO_4 or 0.02M NaCl. To assess the effect of current density (j, mA/cm^2) used in removal experiments, bentazone removal values were studied at 2.4, 4.8, 7.2, and 9.6 mA/cm^2 current densities in 2D/EOP and 3D/EOP reactors containing 0.015 M Na_2SO_4 or 0.02 M NaCl. In 3D/EOP studies, bentazone molecules in the solution can be adsorbed on the surface of the microelectrode with which they are in contact and move away from the solution. Particle electrodes (0.2 g) were used in the experiments to determine the effect of potential difference and j (mA/cm^2) on bentazone removal performance in 3D/EOP. The effect of microelectrode amount in 3D/EOP was determined by experiments performed at 4 V using 0.1, 0.2, 0.3, and 0.4 g 70TEPA/80/6 with Na_2SO_4 and 0.02 M NaCl. We studied the impact of electrolyte concentration on 3D/EOP using various levels of Na_2SO_4 or NaCl: 0.015 M, 0.020 M, 0.030 M, and 0.045 M.

In 3D/EOP, adsorption of bentazone on the surface of particle electrodes enriched with amine groups can occur with electro-oxidation simultaneously. Therefore, adsorption experiments (AD) of bentazone were performed without current using 0.1, 0.2, 0.3, and 0.4 g of 70TEPA/80/6. The degradation efficiency of bentazone was calculated using a formula shown in Eq. 1:

$$\text{Degradation Efficiency } (\varphi) = \frac{C_0 - C_t}{C_0} \times 100 \tag{1}$$

where φ is the degradation efficiency, and C_0 and C_t are the concentration of bentazone at the initial and time t, respectively. The amount of bentazone in the solution that had not undergone oxidation during studies was determined using the Thermo Electron AquaMate UV spectrophotometer (Salman and Hameed 2010). Degradation results are expressed using a 5% error bar. The synergistic effect was evaluated by the synergistic factor, S_f (Eq. 2):

$$S_f = \varphi_{3D/EOP} - (\varphi_{2D/EOP} + \varphi_{AD}) \tag{2}$$

where $\varphi_{3D/EOP}$, $\varphi_{2D/EOP}$, and φ_{AD} are the degradation efficiency or the kinetic constant of 3D/EOP, 2D/EOP, and adsorption, respectively; the greater the S_f is, the stronger the synergistic effect will be.

Additionally, the electrical energy consumed during the process is determined for both 2D/EOP and 3D/EOP reactors using Eq. 3, which calculates E (electrical energy in kWh/m^3) as a function of U (volts), I (current intensity in A), t (time in hours), and V (solution volume in m^3).

$$E = \frac{U.I.t}{V} \tag{3}$$

Energy consumption is also calculated according t (Eq. 4) per unit mass of microelectrodes, where E is electrical

energy (kWh/m^3 g, microelectrodes). Control experiments were not performed.

$$E = \frac{U.I.t}{\text{amount of microelectrode}} \tag{4}$$

Kinetic study

Suppose we view electro-oxidation as a surface treatment. In that case, the rate of degradation can be expressed by the following equation Eq. 5 in terms of the constant of the heterogeneous rate constant, k_h (cm/s) (Kumar et al. 2015).

$$k_h = k_{1\text{or }2,2D\text{ and }3D}\left(\frac{V}{A_e}\right) \tag{5}$$

The surface area of the electrode (A_e) is measured in square centimetres; the reactor volume (V) is measured in cubic centimetres. In the electro-oxidation reactor, the degradation rate of bentazone is proportional to its concentration. The pseudo-first-order and the pseudo-second-order kinetic models, expressed by the following differential equations (Eqs. 6 and 7), are evaluated for the degradation kinetics of bentazone:

$$r = -\frac{d[C]}{dt} = k_{1,2D\text{ or }3D}[C] \tag{6}$$

$$r = -\frac{d[C]}{dt} = k_{2,2D\text{ or }3D}[C]^2 \tag{7}$$

where $k_{1,2D\text{ or }3D}$ and $k_{2,2D\text{ or }3D}$ are the pseudo-first-order reaction rate constant (min^{-1}) and the pseudo-second-order reaction rate constant (cm^3/mol min), respectively; C (mol/cm^3) is the amount of concentration at any time t (t, min).

By integrating Eqs. 6 and 7 over the boundary conditions $t = 0$ and $t = t$ and $C = C_0$ and $C = C$ and then rearranging the equations of interest, the following linear relations was obtained by the pseudo-first-order and the pseudo-second-order kinetic models, respectively.

$$-\ln\left(\frac{C}{C_0}\right) = k_{1,2D\text{ or }3D}t \tag{8}$$

$$\frac{1}{C} - \frac{1}{C_0} = k_{2,2D\text{ or }3D}t \tag{9}$$

The rate constants $k_{1,2D\text{ or }3D}$ and $k_{2,2D\text{ or }3D}$ were determined by plotting $-\ln\left(\frac{C}{C_0}\right)$ and $\left(\frac{1}{C} - \frac{1}{C_0}\right)$ against t.

ANN modelling

Artificial neural network (ANN) entails complicated computations and mathematics that mimic human brain processes. Similar to the structure of the human brain, the ANN models consist of neurons interconnected to each other in a complex form.

Experimental data for ANN modelling employed in this study were obtained by carrying out all the experimental data of 2D and 3D electro-oxidation process for each electrolyte, i.e. Na_2SO_4 and NaCl and computations were performed by MATLAB (R2018b) software. A feed-forward neural network is composed basically of a three-layer network, i.e. input process variables (applied potential difference, current density, particle electrode amount, supporting electrolyte concentration, and pH for each electrolyte), hidden, and output layer (degradation efficiency %) with a purelin function, respectively (Hajiahmadi et al. 2022). The degradation efficiency obtained from the experimental runs was randomly split into training (70%), testing (15%), and validation (15%).

The ANN architectural network in this study included five input variables as the input layers, varying numbers of neuron in the hidden layer with a tan-sigmoid transfer function and an output layer function as shown in Figure S1. The optimum number of hidden nodes was determined by calculating the number of nodes in the hidden layer varying from 1 to 30. Coefficient of determination (R^2) and mean absolute error (MAE) (Eqs. 10 and 11) were used to evaluate the best appropriate model for studying the bentazone degradation (Sridevi et al. 2023). The optimum number of hidden nodes was selected by calculating the lowest MSE. In contrast, a high value of R^2 was used to make accurate predictions and to provide a rational explanation of the experimental data.

$$R^2 = 1 - \frac{\sum_{i=1}^{n}\left[y_{i,\text{experimental}} - y_{i,\text{predicted}}\right]^2}{\sum_{i=1}^{n}\left[y_{i,\text{experimental}} - y_{i,\text{average}}\right]^2} \tag{10}$$

$$MSE = \frac{1}{n}\sum_{i=1}^{n}\left[y_{i,\text{experimental}} - y_{i,\text{predicted}}\right]^2 \tag{11}$$

In the above equations, y represents the degradation efficiency and n denotes the number of experimental datasets.

Following determining the optimum numbers of neurons, the weights of the best suitable neural network were used to assess the relative importance of input variables on output by employing the Garson equation (Eq. 12).

$$I_j = \frac{\sum_{l=1}^{l=N_h}\left[\left(\frac{|W_{kl}^{ih}|}{\sum_{k=1}^{N_i}|W_{kl}^{ih}|}\right)x|W_{kl}^{ih}|\right]}{\sum_{k=1}^{k=N_i}\left[\sum_{l=1}^{l=N_h}\left(\frac{|W_{kl}^{ih}|}{\sum_{k=1}^{N_i}|W_{kl}^{ih}|}\right)x|W_{lm}^{i_k}|\right]} \times 100(\%) \tag{12}$$

where I_j is the relative importance of the input variables on the output, and N_i and N_h are the number of neurons in the input and hidden layers, respectively. Indices of i, h, and o represent the input, hidden, and output layers, respectively,

while k, l, and m represent the input, hidden, and output neurons, respectively (Garson 1991; Nam et al. 2023).

Results

Characterization of C/AC and *TEPA*/ACs

The BET analysis method helps determine porous solids' pore volumes and properties. The pore properties of C/AC and TEPA grafted samples were determined using the BET analysis method. The results are shown in Table 3.

Based on BET analysis, the commercial activated carbon boasts a surface area of 763 m^2/g and a total pore volume of 0.624 cm^3/g. It features a combination of micropores and mesopores, making it an ideal material for studying the impact of TEPA modification on pore structure. The BET results of the C/AC and TEPA/AC samples show that TEPA grafting significantly impacted the porous structure. The surface area of the C/AC sample decreased from 763 m^2/g to 325, 296, and 328 m^2/g for the 20, 50, and 70 TEPA/80/6 samples, respectively; similarly, both micropore and mesopore volumes were also reduced. However, it is important to note that the TEPA grafting had a greater effect on the micropore structures than the mesopore structures. The reduction in micropore volumes is more significant than the decrease in mesopore volumes. The micropore ratio of the C/AC sample was 45.35%, while the micropore ratios of the 20TEPA/80/6, 50TEPA/80/6, and 70TEPA/80/6 samples decreased to 39.04%, 37.05%, and 43.92%, respectively. Additionally, mesopore ratios increased from 54.64 to 60.96%, 62.95%, and 56.08%, respectively, which led to an expansion of the average pore diameters of the samples. These results suggest that TEPA grafting changed the porous structure of activated carbon, with a greater impact on micropore structures. Whang et al. conducted a study on the impact of 50% and 30% TEPA by mass on modifying the MCM41/silica gel mixture at 85 °C. They found that TEPA tends to enter small mesopores, which have a high selectivity (Wang et al. 2015). According to the results, modifying activated carbons with TEPA at a concentration of 70 (wt%) and 80 °C for varying periods of time resulted in a decrease in surface area. Specifically, the surface areas decreased to 346 m^2/g, 328 m^2/g, and 316 m^2/g after 2, 6, and 24 h, respectively.

While there was not a change in the micropore volumes, the mesopore volumes decreased slightly from 0.17 to 0.15 cm^3/g with increasing time at 80 °C. These findings are consistent with a study conducted by Liu et al. (2012).

The graphical representation that expresses the relationship between the amounts of molecules adsorbed on the surface of a solid and any pressure P at constant temperature is called 'adsorption isotherm'. When the adsorbate is vapour, it is preferred to express it in terms of relative vapour pressure (P/P^0) rather than P pressure. Here P^0 is the saturation vapour pressure. Information about the pore shapes and size of a porous solid sample can be obtained by analysing the shapes of the isotherms. IUPAC has classified various solids based on the relationship between their gas adsorption–desorption curves' shapes and their pore structures.

The isotherms for the C/AC sample and samples with different amounts of TEPA modifications for 6 h, as well as samples treated with 70 (wt%) TEPA for 2, 6, and 24 h, are depicted in Fig. 1a, b. These isotherms comply with type I and type IV classifications as per IUPAC standards. In this type of isotherm, the adsorption process starts at relative pressures higher than 0.1, and hysteresis occurs due to capillary condensation in the mesopores as the isotherm continues. This is because the solid contains both mesopores and micropores. The adsorption–desorption isotherms feature H4 type hysteresis, which is common in porous solids with micro- and mesopores. The hysteresis in the C/AC sample is wider than that in TEPA/ACs, primarily due to the C/AC containing more mesopores (Gottipati and Mishra 2016; Üner and Bayrak 2018).

Many adsorbents have varying widths, lengths, and diameters in their pore structures. These pores may have connections to each other and openings on the outer surface, with sizes and shapes differing from solid to solid. The pore size distributions of C/AC and 20, 50, and 70TEPA/80/6 are displayed in Fig. 1c. C/AC displays peaks between 10–20 Å (1–2 nm) and 20–60 Å (2–4 nm). All samples modified with different concentrations of TEPA at 80 °C have similar pore size distributions in

Table 3 Features of porous surface structures of C/AC and TEPA/ACs

ID	S_{BET} (m^2/g)	V_{mic} (cm^3/g)	V_{mes} (cm^3/g)	V_{tot} (cm^3/g)	$\frac{V_{mic}}{V_{tot}}\times100$	$\frac{V_{mes}}{V_{tot}}\times100$	D_p (Å)
C/AC	763	0.283	0.341	0.624	45.35	54.64	3.247
20TEPA/80/6	325	0.11	0.18	0.29	39.04	60.96	3.60
50TEPA/80/6	296	0.10	0.18	0.28	37.05	62.95	3.76
70TEPA/80/6	328	0.11	0.14	0.26	43.92	56.08	3.60
70TEPA/80/2	346	0.12	0.17	0.30	41.41	58.59	3.43
70TEPA/80/24	316	0.11	0.15	0.27	41.89	58.11	3.36

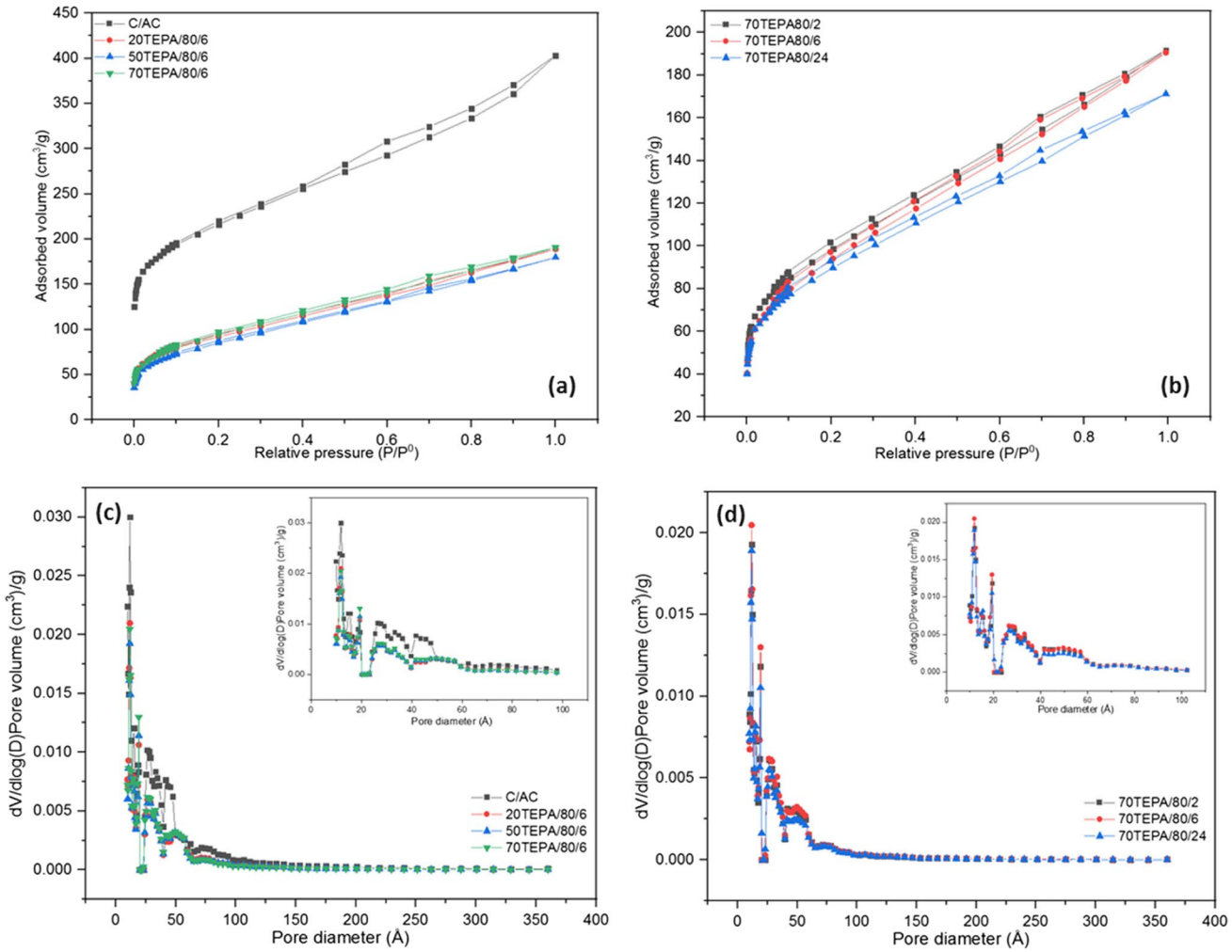

Fig. 1 N_2 adsorption–desorption isotherms (**a**, **b**) and pore size distributions (**c**, **d**) of C/AC and TEPA/ACs

micropore and mesopore areas. Therefore, increasing TEPA concentration at high temperatures does not alter the pore size distributions. Additionally, Fig. 1d shows that all samples modified for 2, 6, and 24 h at a TEPA concentration of 70 (wt%) at 80 °C had peaks in the micro- and mesopore areas, and the peaks of the three samples overlapped. Therefore, increasing the time at high TEPA concentrations and temperatures does not significantly impact pore widths. FTIR images of C/AC and TEPA/ACs are given in Fig. 2a–c.

The band seen at 3408 cm^{-1} in the FTIR spectrum of C/AC given in Fig. 2c is attributed to the vibrations of hydrogen-bonded hydroxyl groups (Momcilovic et al. 2011). It is related to the stretching vibration of the C = C bond of the aromatic ring formed at 1563 cm^{-1} (Guo and Rockstraw 2007; Qu et al. 2007). The 1169 cm^{-1} and 798 cm^{-1} peaks are C-O and C-H tension vibrations, respectively (Fig. 2c) (Deng et al. 2009; Liou 2010).

When analysing the spectra in Fig. 2 a and b of the modified activated carbons, similar peaks are observed. The band seen in the spectra of the samples between 3420 and 3273 cm^{-1} is associated with the -OH and N–H tension vibration in the amine-treated samples. The peak at ~ 2910 cm^{-1} is due to the symmetrical and asymmetric vibration of the -C-H bond (Fig. 2 a and b). In addition, the -NH and N–H groups in the structure of TEPA molecules attached to the surface of the modified carbons were confirmed by the bands seen between 1786 and 1679 cm^{-1} and between 1623 and 1386 cm^{-1}, respectively. The band between 1386 and 1015 cm^{-1} is associated with C-N bond vibration (Jiang et al. 2012; Abd El-Magied et al. 2018; Tang et al. 2018; Rajasekaran et al. 2021).

First, the surface of the activated carbons underwent an acid functional group enrichment process using HNO_3 before TEPA grafting. The amount of acidic functional groups present on the surface was determined using the Boehm method. Once TEPA modification occurred and TEPA

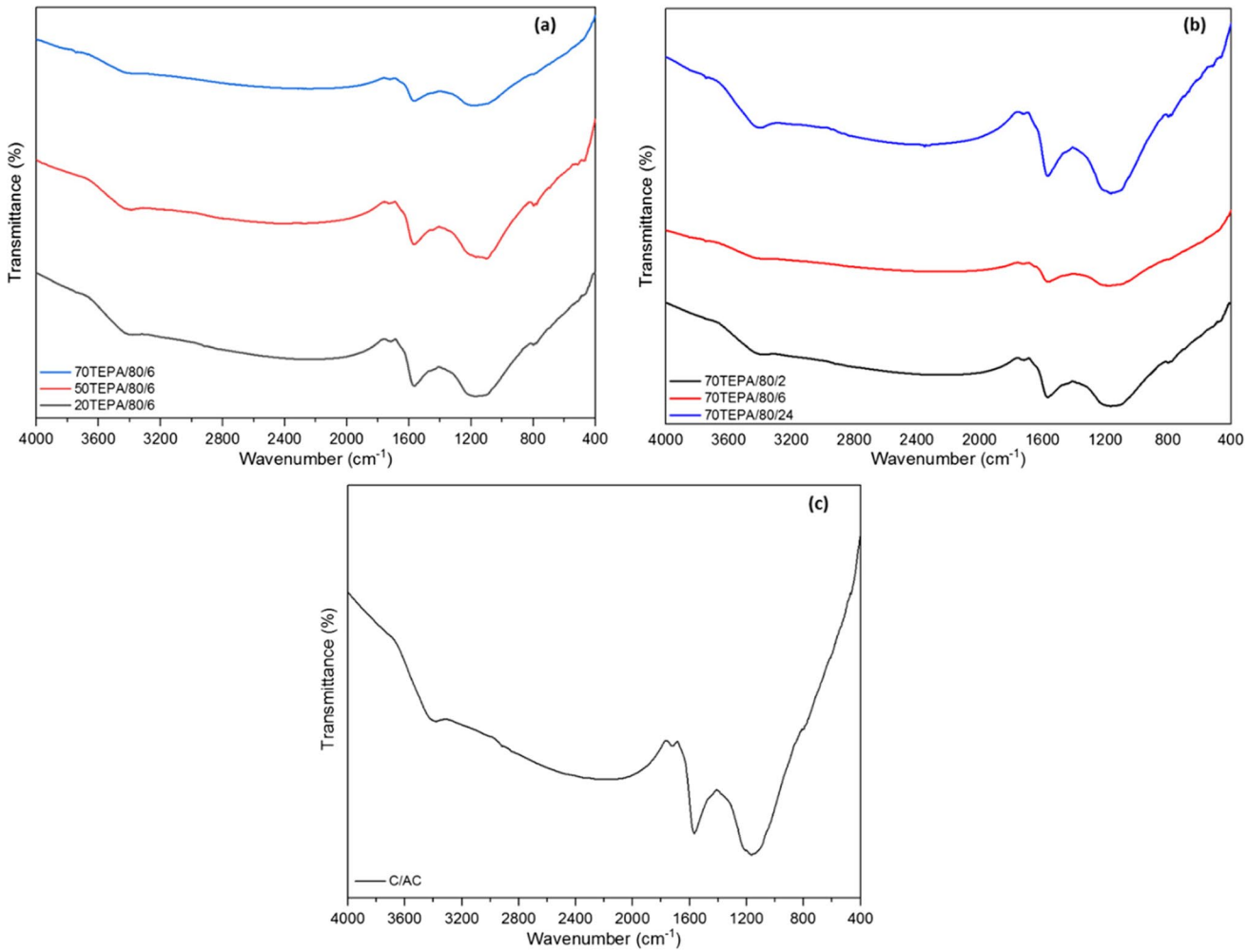

Fig. 2 FTIR spectra of TEPAs (**a**, **b**) and C/AC (**c**)

molecules were grafted onto the surface, the amount of acidic functional groups decreased while basicity increased. Table 4 displays the amounts of certain functional groups found on the surface of TEPA/ACs, which were determined using the Boehm method.

According to Boehm titration results of acidified C/AC, 2.40 mmol/g carboxylic, 2.20 mmol/g lactone, and 3.02 mmol/g phenolic species are found on the surface of nitric acid–modified activated carbon. While the total acidity value was 7.62 mmol/g, the total basicity value was determined as 0.1 mmol/g. Strong base amine group–containing TEPA molecules were grafted onto the acidic surface. With the addition of 20% (wt)TEPA by mass, the total basicity value of acidified C/AC increased from 0.1

Table 4 Boehm titration results of acidified C/AC and TEPA/ACs

	Total base (mmol/g)	Total acidity (mmol/g)	Carboxyl (mmol/g)	Lactones (mmol/g)	Phenol (mmol/g)
Acidified C/AC	0.1	7.62	2.40	2.20	3.02
20TEPA/80/6	3.05	0.88	0.35	0	0.53
50TEPA/80/6	4.05	0	0	0	0
70TEPA/80/6	4.35	0	0	0	0
70TEPA/80/2	3.05	1.02	0.62	0.35	0.05
70TEPA/80/6	4.35	0	0	0	0
70TEPA/80/24	3.87	0	0	0	0

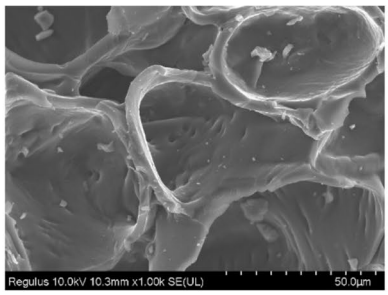
Regulus 10.0kV 10.3mm x1.00k SE(UL)
50.0µm

(a)

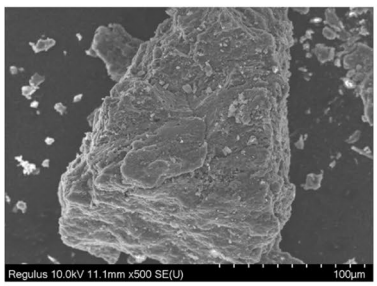
Regulus 10.0kV 11.1mm x500 SE(U)
100µm

(b)

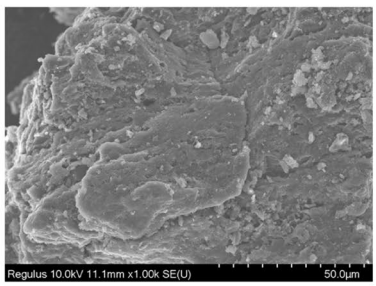
Regulus 10.0kV 11.1mm x1.00k SE(U)
50.0µm

(c)

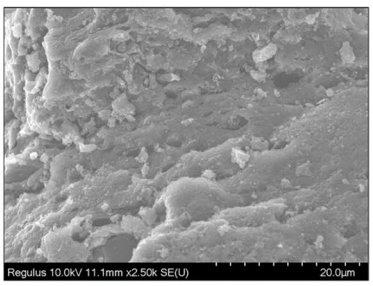
Regulus 10.0kV 11.1mm x2.50k SE(U)
20.0µm

(d)

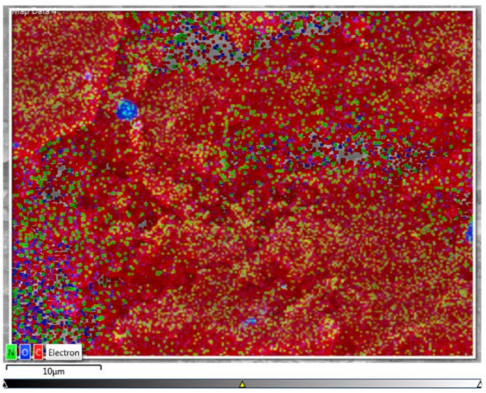
Electron
10µm

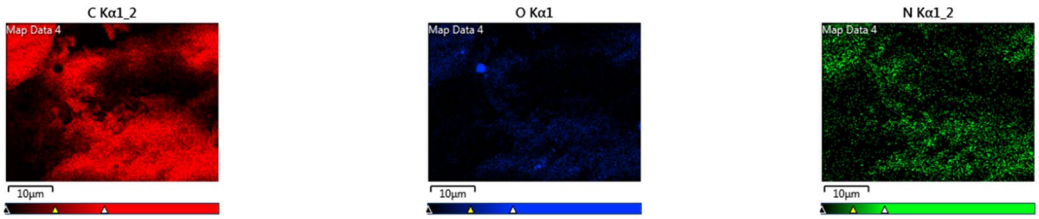
C Kα1_2
Map Data 4
10µm
O Kα1
Map Data 4
10µm
N Kα1_2
Map Data 4
10µm

(e)

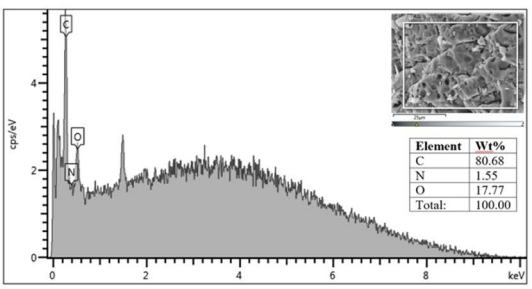
C
O
N
cps/eV
keV
Element Wt%
C 80.68
N 1.55
O 17.77
Total: 100.00

(f)

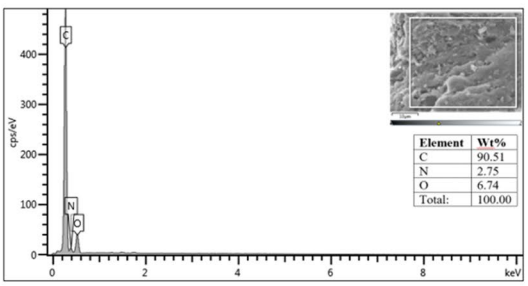
C
N
O
cps/eV
keV
Element Wt%
C 90.51
N 2.75
O 6.74
Total: 100.00

(g)

◂**Fig. 3** SEM micrographs of C/AC at 2500 × magnification (**a**) and 70TEPA/80/6 at 500 × magnification (**b**), 70TEPA/80/6 at 1000 × magnification (**c**), 70TEPA/80/6 at 2500 × magnification (**d**), EDS layered image of 70TEPA/80/6 (**e**), and EDS analysis results of acidified C/AC (**f**) and 70TEPA/80/6 (**g**)

to 3.05 mmol/g, while the total acidity value decreased to 0.88 mmol/g. Moreover, the TEPA molecules attached to the acidified C/AC surface reduced the amount of carboxyl, lactone, and phenol on the surface to 0.35, 0, and 0.53 mmol/g, respectively. The grafted TEPA molecules showed a preference for phenol > lactone > carboxyl groups, respectively.

After the grafting process was performed under various conditions, all TEPA-modified samples had a lower acidity value compared to the total acidity value of the acidified C/AC surface. These findings indicate that amine groups were successfully grafted onto the activated carbons' surface in all of the studied TEPA modification conditions.

As more TEPA was used in the 6-h grafting process, an increased amount of basic functional groups formed on the surface of TEPA/ACs. For instance, 70TEPA/80/6 displayed a total alkalinity value of 4.35 mmol/g, whereas 20TEPA/80/6 exhibited a total alkalinity value of 3.05 mmol/g. This indicates that the concentration of TEPA utilized during the grafting process plays a critical role.

The surface functional group amounts were compared after modifying activated carbons for 2, 6, and 24 h using 70% (wt) TEPA. It was found that increasing the inoculation time from 2 to 6 h increased total alkalinity value from 3.05 to 4.35 mmol/g. However, inoculating for 24 h harmed the amount of TEPA molecules grafted onto the surface. The best results were achieved by using 70% (wt) TEPA by mass in the grafting process for 6 h, as revealed by the Boehm results. The results of SEM analysis for C/AC and 70TEPA/80/6 and EDS analysis results for acidified C/AC and 70TEPA/80/6 are shown in Fig. 3 (a–f).

From the SEM image in Fig. 3 (a) at 1000 × magnification, the porous surface of the C/AC is visible. Upon examining the SEM images of 70TEPA/80/6 at 500 ×, 1000 ×, and 2500 × magnifications, it is apparent that the surfaces are less porous (Fig. 3 (b–d)). This can be attributed to the TEPA molecules grafted onto the surface of C/AC, disrupting its porous structure.

Based on the colour of the elements on the surface, it is possible to predict the distribution of TEPA molecules bound to the C/AC surface. Figure 3 (e) shows the elemental map of the top surface layer of 70TEPA/80/6. TEPA molecules are composed of C, H, and N atoms. For this reason, the distribution on the surface can be seen by looking at the N atoms in the TEPA molecules grafted onto the 70TEPA/80/6 surface. The elemental mapping shows C atoms in red and N atoms in green. The green-coloured dots scattered throughout the picture show that TEPA has been grafted onto many parts of the activated carbon surface.

According to the EDS analysis (Fig. 3 (f–g)), acidified C/AC consists of C 80.68%, N 1.55%, and O 17.77%. The modified carbon surface consists of C 90.51%, O 6.74%, and N 2.75%. The presence of TEPA molecules grafted onto the carbon surface led to an increase in its carbon and nitrogen content while causing a decrease in the oxygen content due to reduced oxygen-containing functional groups. These results show that the TEPA was successfully grafted onto the surface.

Determination of electrochemical properties of carbon fibre electrode

Cyclic voltammetry was used to analyse the electrochemical activity of carbon fibre in a three-electrode configuration with NaCl and Na_2SO_4 solutions. The results are presented in Fig. 4 a and b.

When Fig. 4a is examined, a concave curve shows that there are reduction–oxidation reactions on the surface at potential differences lower and higher than − 0.5 V at a scanning speed of 10 mV/s. However, it was observed that the concave curve disappeared when the scanning rate was increased from 10 to 100 mV/s. As the scanning speed increased, the residence time of the molecules transported to the surface of the carbon fibre decreased. Not enough time may have prevented the reaction from occurring.

When examining Fig. 4b, it is evident that there are concave curves which indicate the occurrence of reduction–oxidation reactions on the surface of carbon fibre at scanning speeds ranging from 10 to 100 mV/s and potential differences lower than 1 mV. If NaCl is present in the solution, the oxidative system can lead to the formation of reactive chlorine species. The transfer of electrons from chloride results in the formation of Cl_2, which reacts with ·OH. Furthermore, Cl_2 and H_2O react to produce HOCl, which can cause concave curves (Szpyrkowicz et al. 2005; Wu et al. 2019, 2021).

Degradation and adsorption studies

The degradation of bentazone through electrochemical processes in two-dimensional and three-dimensional electro-oxidation systems may involve various mechanisms. In both types of systems, applying an electric field leads to the oxidation of bentazone molecules on the electrode surface. This oxidation generates reactive oxygen species (ROS) that interact with bentazone, transforming it into more straightforward and less harmful byproducts. The production of electrogenerated reactive oxygen species, such as hydroxyl radicals (•OH) and ozone (O3), significantly contributes to the degradation of bentazone. These reactive species can disrupt the chemical structure of bentazone, breaking its

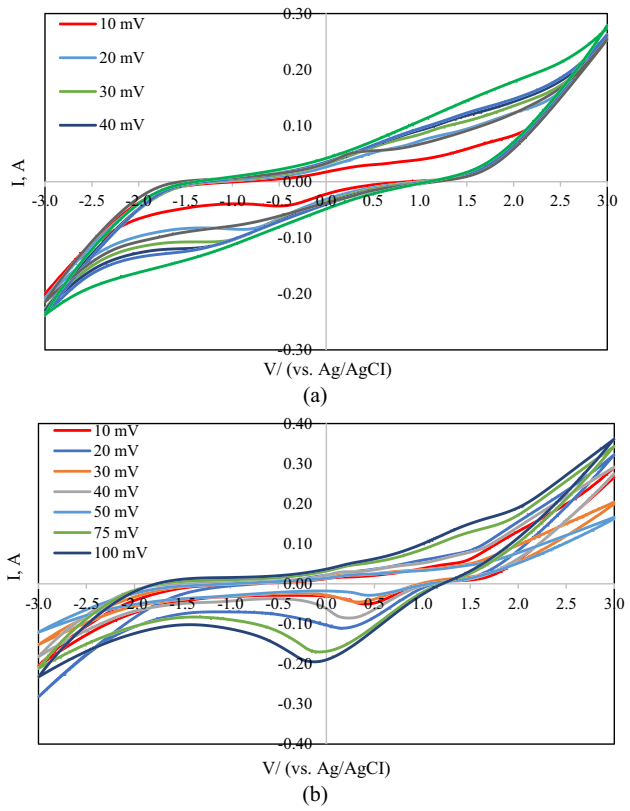

Fig. 4 Cyclic voltammetry (CV) measurements (vs. Ag/AgCl) in the − 3 to 3 V potential window at a scan rate of 10, 20, 30, 40, 50, 75 and 100 mV/s in Na_2SO_4 (**a**) and NaCl (**b**)

bonds and converting it into less complex and less toxic compounds. The pH of the electrolyte solution also has an impact on bentazone degradation in electro-oxidation systems. Changes in pH can affect the production and reactivity of ROS, as well as bentazone molecules' stability, ultimately influencing degradation efficiency. Apart from direct oxidation at the electrode surface, indirect oxidation reactions can occur in both two-dimensional and three-dimensional electro-oxidation systems. These reactions involve the creation of secondary oxidants or radical species that may contribute to the degradation of bentazone.

Effect of voltage

The applied potential difference is critical to enhance the degradation efficiency of bentazone during electro-oxidation in various electrolyte solutions. The potential difference controls the rate of electron transfer and oxidation reactions required to dissociate bentazone molecules. Figure 5 a–d show the effect of voltage on decomposition efficiency percentage and normalized concentration in Na_2SO_4 and NaCl solutions, respectively.

The effect of bentazone degradation in Na_2SO_4 and NaCl solutions was positively influenced by the applied potential difference in the reactors. In the Na_2SO_4 solution, increasing the potential difference from 4 to 7 V resulted in a slight rise in degradation efficiency from 20.68 to 26.03% in 2D/EOP. However, a similar increase in the potential difference in 3D/EOP led to an increase in degradation efficiency from 35.74 to 78.71% (Fig. 5a). The normalized concentration decreased from 0.76 to 0.74 in 2D/EOP and from 0.64 to 0.21 in 3D/EOP with an increase in potential difference from 4 to 7 V (Fig. 5c). In the NaCl solution, increasing the potential difference led to an increase in degradation efficiency from 49.53 to 63.51% in 2D/EOP and from 76.80 to 81.66% in 3D/EOP (Fig. 5b). Similarly, the normalized concentration decreased from 0.50 to 0.36 in 2D/EOP and from 0.23 to 0.18 in 3D/EOP (Fig. 5d).

When potential differences are applied, the degradation efficiency in 3D/EOP reactors is higher compared to 2D/EOP reactors. The formation of oxidizing species in a solution can be the reason for this occurrence in the 2D/EOP and 3D/EOP. The OH* radicals are considered the most potent oxidizing agent ($E^{\circ} = 2.80$). When more potential differences are applied to electrochemical oxidation systems, the formation of OH* radicals happens, which directly oxidizes the anode surface (Kumar et al. 2014; Chen et al. 2019). While bentazone oxidation mainly occurs through direct oxidation on the carbon fibre electrode surface, it also occurs with weak oxidizing species formed in the solution as the potential difference increases (Costa et al. 2009; Kumar et al. 2014; Cho et al. 2020). Direct oxidation occurs at the electrode's surface while indirect oxidation involves the anodic generation of oxidants like H_2O_2, Cl_2, HClO, or hydroxyl radicals produced by water electrolysis.

Additionally, 70TEPA/80/6 serves as a catalyst for converting H_2O_2 to OH radicals, which leads to a significant increase in the favourable radical in 3D/EOP systems compared to 2D systems. The high conductivity of 70/TEPA/80/6 also plays a charged microelectrode role under an induced electric field, enhancing pollutant direct oxidation and decreasing migration distance (Chen et al. 2019; Foroughi et al. 2020).

In their study in which they examined the electrochemical degradation of 2-diethylamino-6-methyl-4-hydroxypyrimidine using a three-dimensional reactor with ceramic particle electrodes, Li et al. determined that the interference efficiency increased with the voltage applied to the cell, reaching a maximum value at 15 V. They stated that this is because the higher cell voltage can produce higher driving force for the repolarization of the particle electrodes (Li et al. 2015).

In their study investigating the effect of nitrogen-doped reduced graphene oxide on tetracycline degradation in a three-dimensional electrode reactor, Liu et al. determined

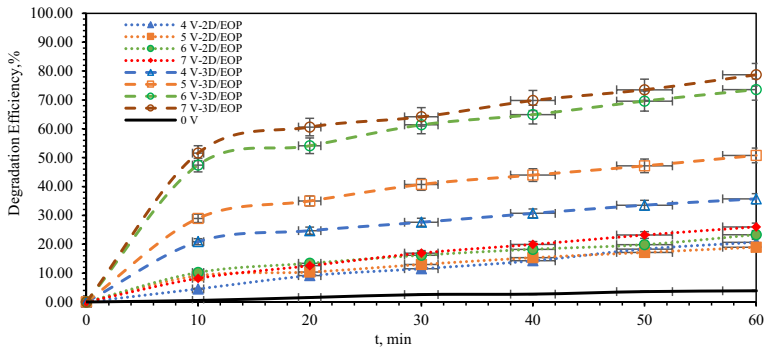

(a)

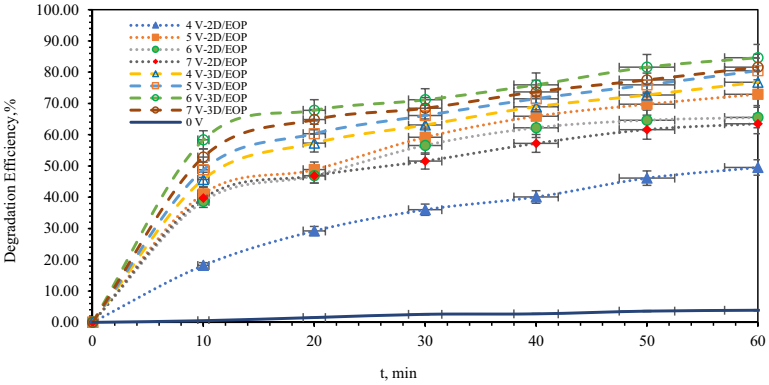

(b)

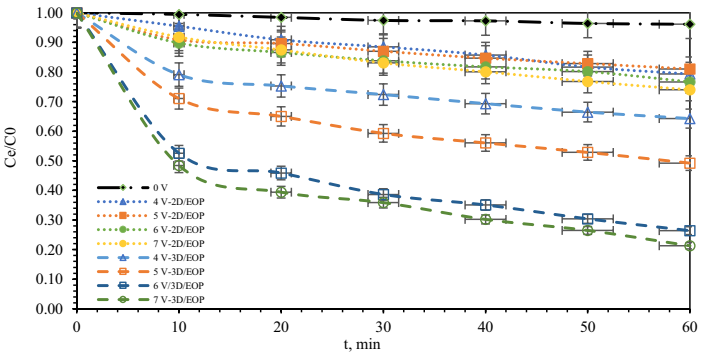

(c)

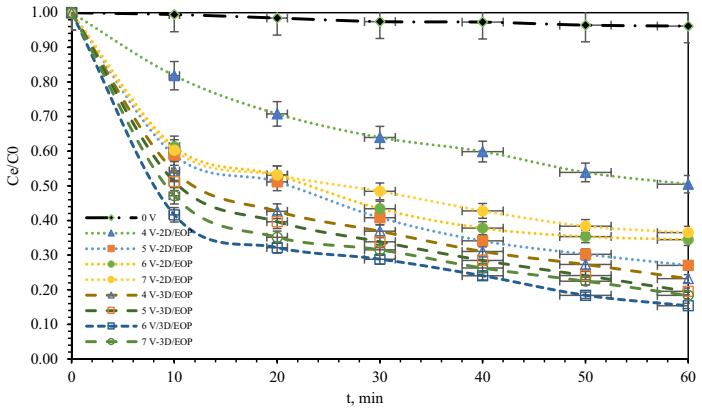

(d)

Fig. 5 Voltage effect on the degradation efficiency of bentazone in 2D/EOP and 3D/EOP. Degradation efficiency (%) against time for 0.015 M Na_2SO_4 (**a**) and 0.02 M NaCl (**b**). Normalized concentration of bentazone against time for 0.015 M Na_2SO_4 (**c**) and 0.02 M NaCl (**d**)

that tetracycline degradation increased from 78 to 90.2% when the voltage was increased from 2 to 4 V. They stated that this situation is due to the increase in catalytic reactions and adsorption in the system with the increase in electron transfer in solution (Liu and Zhang 2024).

The adsorption mechanism is expected to activate when the reactor is not under voltage and 70TEPA/80/6 are present in the system. However, during 60 min, this mechanism only removed 3.87% of the 100 ppm bentazone. The negative charges of TEPA can ionize under the potential difference on the surface of the 70TEPA/80/6 in the 3D/EOP, which causes the bentazone to condense on the surface of the microparticles. Bentazone can be directly oxidized at the microelectrode-solution interface without the adsorption of bentazone to the active points of TEPA (Zheng et al. 2016). Therefore, using microelectrodes charged under current provides a higher bentazone removal efficiency in the 3D/EOP.

Similar results were obtained with the study results, in which Ji and colleagues investigated the optimization of multiple responses to efficiently treat rhodamine B wastewater in a three-dimensional electrochemical reactor focused on energy saving. They observed that the applied voltage largely influences the extent of direct oxidation on both the main and particle electrodes. They indicated that the voltage impacts the electrode potential of the main electrodes, leading to increased oxidation of contaminants. Additionally, they proposed that the voltage also affects the polarization behaviour of the particle electrodes, resulting in increased direct oxidation at these electrodes. They highlighted the significant role of the applied voltage in the generation of oxidizing species (e.g. H_2O_2, Cl_2, HClO) and its contribution to the removal of pollutants through indirect oxidation (Ji et al. 2018b).

Effect of current density (j)

In electrochemical wastewater treatment, optimizing the current density is crucial as it impacts the removal of pollutants and capital costs. To investigate how current density affects the degradation of bentazone solution in 3D/EOP and 2D/EOP reactors, we tested various current densities (*j*): 2.4, 4.8, 7.2, and 9.6 mA/cm^2. All other conditions remained constant, including an initial bentazone concentration of 100 ppm, Na_2SO_4 concentration of 0.015 M or NaCl concentration of 0.02 M, and a carbon fibre surface of 6.25 cm^2. Figure 6 a–d depict how changing the current density (*j*) in 2D/EOP and 3D/EOP reactors impacts the bentazone degradation efficiency and normalized (C/C_0) concentration in two different supporting electrolytes.

Based on the findings, it is evident that a higher current density has a positive impact on both the 2D/EOP and 3D/EOP (Fig. 6a, b). The most significant impact was seen in both oxidation reactors, significantly when the current density (*j*) rose to 4.8 mA/cm^2 in the Na_2SO_4 supporting electrolyte. In the 2D/EOP with the Na_2SO_4 supporting electrolyte, the degradation efficiency of bentazone increased from 32.05 to 40.33% when the *j* increased from 2.4 to 4.8 mA/cm^2. Meanwhile, the efficiency in 3D/EOP was changed from 50.75 to 63.13%. Moreover, as the *j* increased, the degradation efficiency in 2D and 3D EOPs rose, reaching 55.29% and 69.77%, respectively, when the *j* was 9.6 (Fig. 6a). When the *j* increased from 2.4 to 9.6, the normalized concentration decreased from 0.68 to 0.45 in 2D/EOP, while in 3D reactors, it decreased from 0.49 to 0.30 (Fig. 6c).

When NaCl supporting electrolyte was present, an increase in the *j* had the most significant impact on the degradation of bentazone in 3D/EOP reactors. Increasing the *j* from 2.4 to 7.2 mA/cm^2 resulted in a 14.75% increase in efficiency, reaching 50.06% in 2D/EOP. In 3D/EOP, the efficiency increased by 25.64% and reached 87.49%. When NaCl supporting electrolyte was used, as the *j* increased, the normalized concentration decreased from 0.65 to 0.44 in 2D reactors, while it decreased from 0.38 to 0.08 in 3D reactors (Fig. 6d).

As *j* increases, a greater amount of bentazone degradation occurs on both the microelectrode and the carbon fibre electrode surfaces. Additionally, the increase in secondary reactions produces an increase in the number of reactive oxygen species such as OH, H_2O_2, and HClO in the solution, and these oxidizing species lead to more significant bentazone removal through indirect oxidation (Sarkka et al. 2015; Liu et al. 2020; Wu et al. 2021). Increasing the current density to 9.6 mA/cm^2 in 2D and 3D reactors resulted in only slightly improved decay efficiency. This might be because the short circuit and bypass current were increased under higher current density (Zheng et al. 2016).

Xiao et al. and He et al. stated that a current density that is too high should be avoided for several reasons. They also came to the following conclusions regarding high current density. First, it would lead to the anode's hydrogen evolution reaction and the cathode's oxygen evolution reaction. Second, a high current density in a three-dimensional electrode system would cause a high bypass current and short-circuit current, resulting in low current efficiency. Third, the oxygen evolution side reaction would decrease the utilization efficiency of hydroxyl radicals. Finally, the high current density would generate excess heat during electrolysis, reducing energy utilization (He et al. 2014; Xiao and Zhang 2016).

Supporting electrolyte type effect

In electrochemical reactions, the properties of the anode, electrode, and electrolyte, the applied potential, and the factors affecting the course of the electrochemical reaction are essential in the events taking place at the interface. The

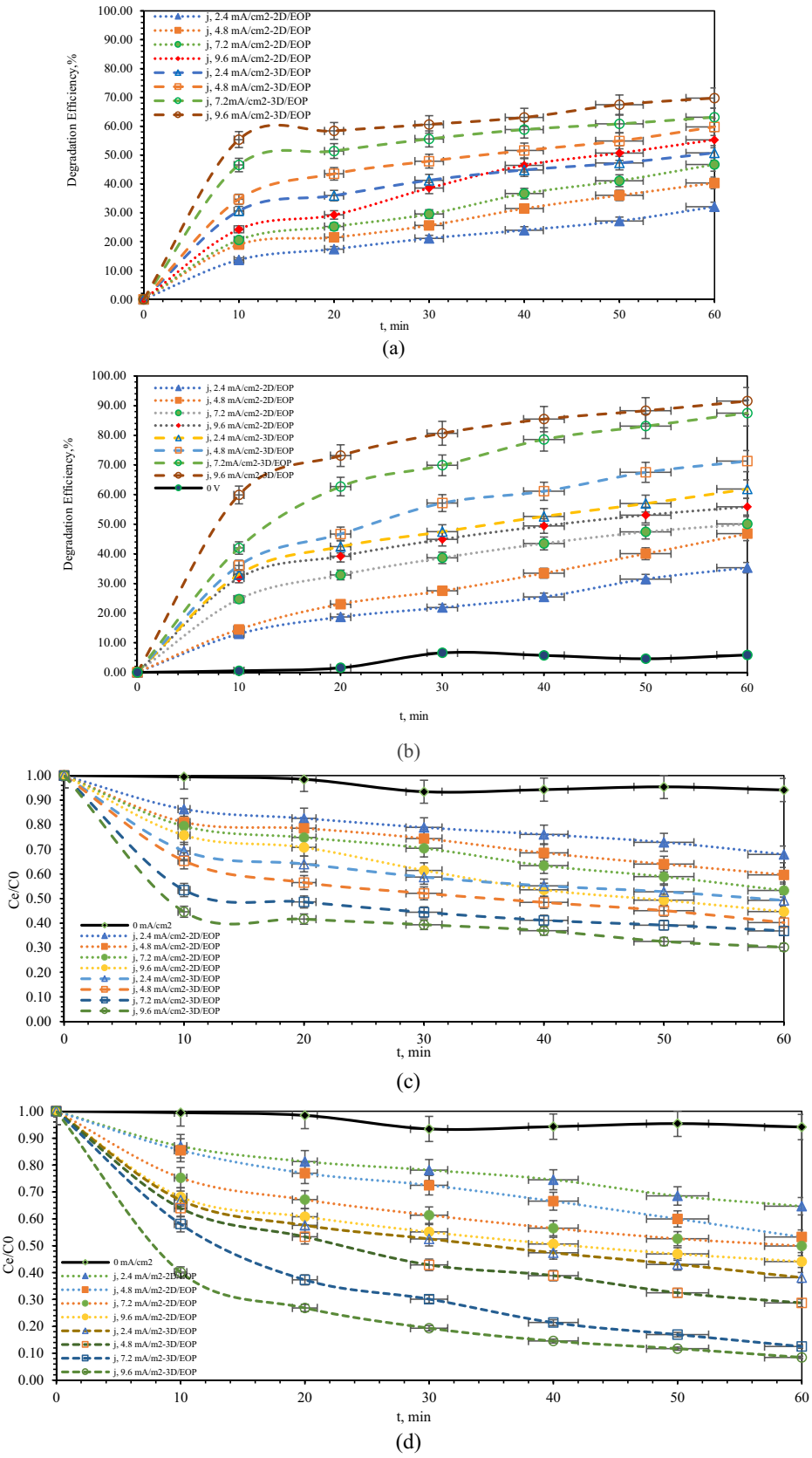

Fig. 6 Current density on the degradation efficiency of bentazone in 2D/EOP and 3D/EOP. Degradation efficiency (%) of bentazone against time for 0.015 M Na_2SO_4 (**a**) and 0.02 M NaCl (**b**). Normalized concentration of bentazone against time for 0.015 M Na_2SO_4 (**c**) and 0.02 M NaCl (**d**)

selection of accompanying electrolytes may impact the efficiency of the electro-oxidation procedure. For instance, the presence of Na_2SO_4 can boost the breakdown of bentazone by elevating conductivity and encouraging the generation of reactive oxygen species. NaCl can substantially influence the degradation procedure, potentially modifying the production of secondary products or impacting the overall reaction rate.

Supporting electrolyte type and concentration affect the removal efficiency of electrochemical processes. Figure 7 a and b show the results of an investigation into the bentazone degradation efficiency and normalized (C/C_0) concentration in 3D/EOPs with varying amounts of Na_2SO_4 and NaCl supporting electrolytes.

In Fig. 7 a and b, it is evident that the degradation of bentazone is directly influenced by the concentration of NaCl and Na_2SO_4. With the increase in concentrations of Na_2SO_4 and NaCl, the efficiency of bentazone degradation also increased. The degradation reached 43.53% in a 0.045-M Na_2SO_4 solution and 92.84% in a 0.045-M NaCl solution (Fig. 7a). As the amount of Na_2SO_4 supporting electrolyte was increased, the normalized concentration value in the 3D reactors changed slightly from 0.64 to 0.56. On the other hand, when NaCl was used as the supporting electrolyte, the normalized concentration value decreased significantly as the amount of supporting electrolyte increased, changing from 0.23 to 0.07 (Fig. 7b). It was observed that the change in NaCl concentration had a significant impact on the degradation process.

Adding a supporting electrolyte boosts the ionic strength of the solution, leading to an increase in its conductivity (Khelifa et al. 2005). A higher concentration of NaCl leads to an increase in the number of active species, namely active chlorine (Cl_2, HClO, and ClO), which facilitate the transfer of electrons between the electrode and the pollutant (Vlyssides et al. 2004). Active chlorine species promote indirect oxidation within the reactor and increase the degradation efficiency of bentazone (Oliveira et al. 2007).

When the Na_2SO_4 support electrolyte is used, weak oxidative species such as $S_2O_8^{-2}$ and SO_4^{-2} are formed in the solution. These species provide the breakdown of organics by indirect oxidation. In our study, it is clear that the increase in the amount of Na_2SO_4 does not support the formation of these weak oxidative species formed in solution. It was determined that the increase in the amount of Na_2SO_4 did not affect the indirect oxidation of bentazone much. Liu et al. obtained similar results to ours in a study they conducted.

Liu et al. studied the effect of persulfate on tetracycline degradation by electrochemically activating persulfate in a three-dimensional electrode reactor. They stated that the increase in persulfate concentration increased the amount of $SO_4^{\cdot -}$ and OH*, thus increasing the removal of tetracycline.

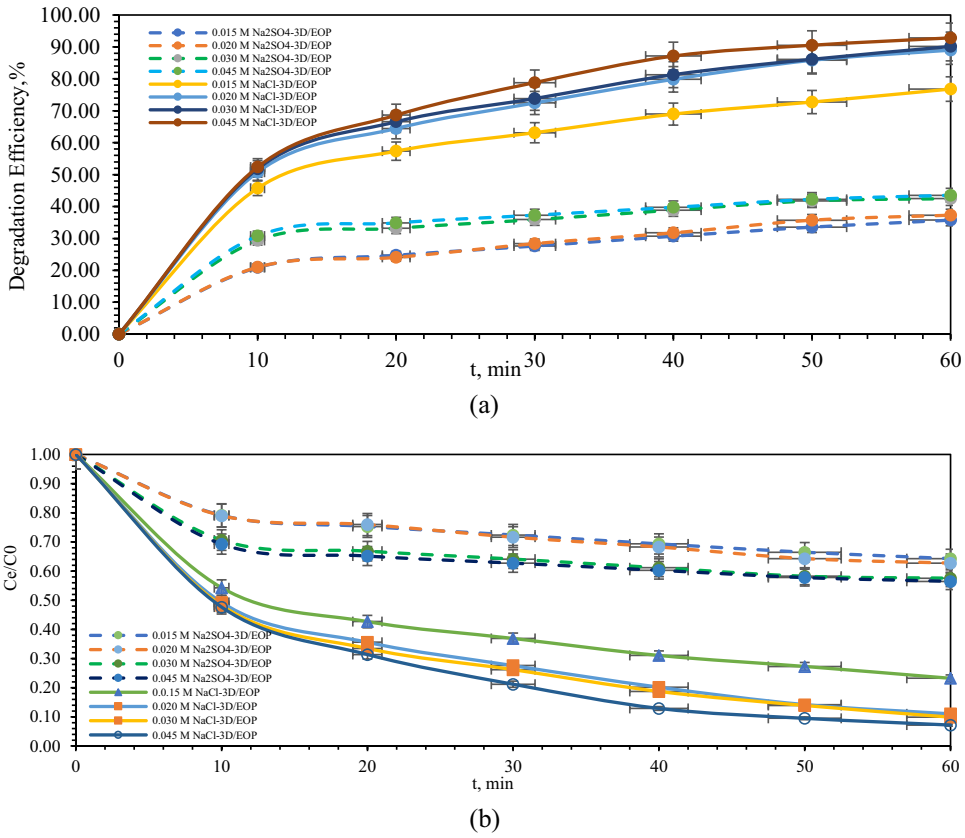

Fig. 7 Relationship between $\ln(C/C_0)$ and supporting electrolyte concentration (**a**) and relationship between bentazone degradation efficiency and supporting electrolyte concentration (**b**)

However, when the concentration of persulfate becomes too high, $SO_4^{\cdot -}$ not only reacts with excess $S_2O_8^{2-}$, but also reacts on its own. They concluded that excessive amounts of persulfate caused self-quenching reactions and adversely affected tetracycline oxidation (Liu and Zhang 2024).

Effect of pH

The pH level is essential during the electrochemical oxidation process as it influences the charge and type of interaction between the oxidation agents and the organic material. Figure 8 demonstrates the impact of pH on the degradation of bentazone in 3A/EOP. The efficiency of bentazone degradation in both electrolyte solutions decreased slightly as the pH increased. The efficiency of bentazone degradation decreased from 61.72% at a pH level of 3 to 59.32% at a pH level of 9 when Na_2SO_4 was used as the supporting electrolyte. In the presence of Na_2SO_4, the pH of the solution had little effect on the degradation efficiency. However, when NaCl was used as the supporting electrolyte, solution pH significantly affected degradation efficiency. At pH 3, a degradation efficiency of 79.59% was achieved, while at pH 9, only 66.26% removal was obtained. This is due to the surface charge of the particle electrodes and the ionic species present in the solution. Bentazone has a pKa value of 3.3, which suggests that bentazone exists as an anion when the pH is above 3.3 (Table 1) (Spaltro et al. 2019; PubChem 2023, p. 3430). In their study investigating the electrochemical determination of bentazone using a carbon nanotube b-cyclodextrin modified electrode, Rahemi et al. determined that the anionic form constituted 83 mol% at pH 4, while it represented more than 99% at pH 6–7. They stated that bentazone was predominantly present in the anionic form under the tested pH conditions (3–8.1) (Rahemi et al. 2013).

When the pH is low, the particle electrodes with TEPA-functionalization degrade bentazone more efficiently. At low pH, the H^+ ions in the environment cause the microelectrode surface to become positively charged through protonation. This causes a stronger attraction between the active sites on the microelectrode surface and the bentazone molecules, leading to increased mass transfer of bentazone ions towards the surface of the particle electrode (Huang et al. 2011). This enhances the direct degradation of bentazone on the microelectrode surface. Wang et al., in their study examining the anodic and indirect cathodic oxidation of colour and COD in textile dyeing wastewater, noted that the increase in the pH of the environment led to an increase in oxygen release and a decrease in the amount of removal (Wang et al. 2009).

In the presence of Cl_2 at low pH, $HClO^*$ ($E^\circ = 1.49$ V/SHE) is formed according to Eq. 30. Therefore, the presence of species with high reduction potential in solution at low pH increases the efficiency of bentazone degradation in 3D/EOP (Szpyrkowicz et al. 2005; Wu et al. 2021). In their study investigating the decontamination of wastewater containing synthetic organic dyes using electrochemical methods, Martínez-Huitle and Brillas stated that when NaCl was dosed as an electrolyte, the soluble chlorine produced at the anode was rapidly hydrolysed to HClO, leading to the mineralization of RhB (Martínez-Huitle and Brillas 2009).

Effect of particle electrode amount

The degradation efficiency of the 3D/EOP was evaluated under various microelectrode dosages (0.1–0.4 g). Particle electrodes can adsorb bentazone molecules simultaneously with oxidation. For this reason, adsorption experiments were carried out using different TEPA/80/6 dosages; the results are presented in Fig. 9 (Zheng et al. 2016). Figure 9 a–d show the results of an investigation into the bentazone degradation efficiency and normalized (C/C_0) concentration in 3D/EOPs with varying amounts of particle electrodes in Na_2SO_4 and NaCl supporting electrolytes.

Particle electrodes showed little adsorption capacity for bentazone. It can be said that bentazone degradation in 2D/EOP and 3D/EOP occurs by electrochemical mechanisms.

When a 4V potential difference was applied to 2D/EOP, only 20.68% and 49.53% bentazone removal occurred in the presence of Na_2SO4 and NaCl supporting electrolytes,

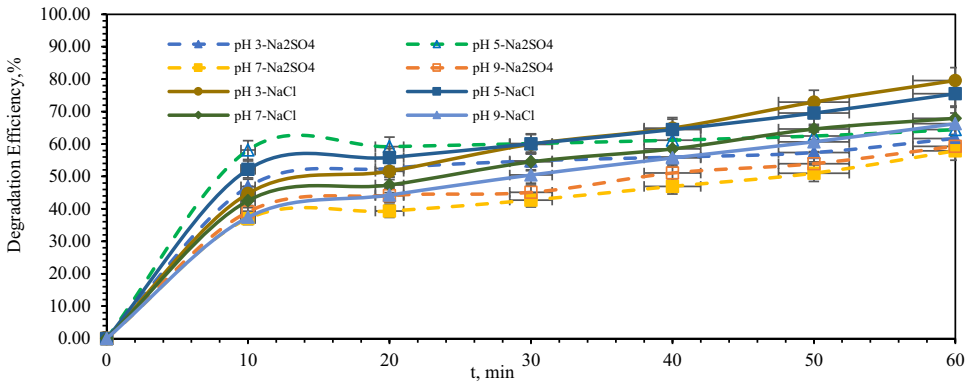

Fig. 8 Effect of pH on bentazone degradation efficiency

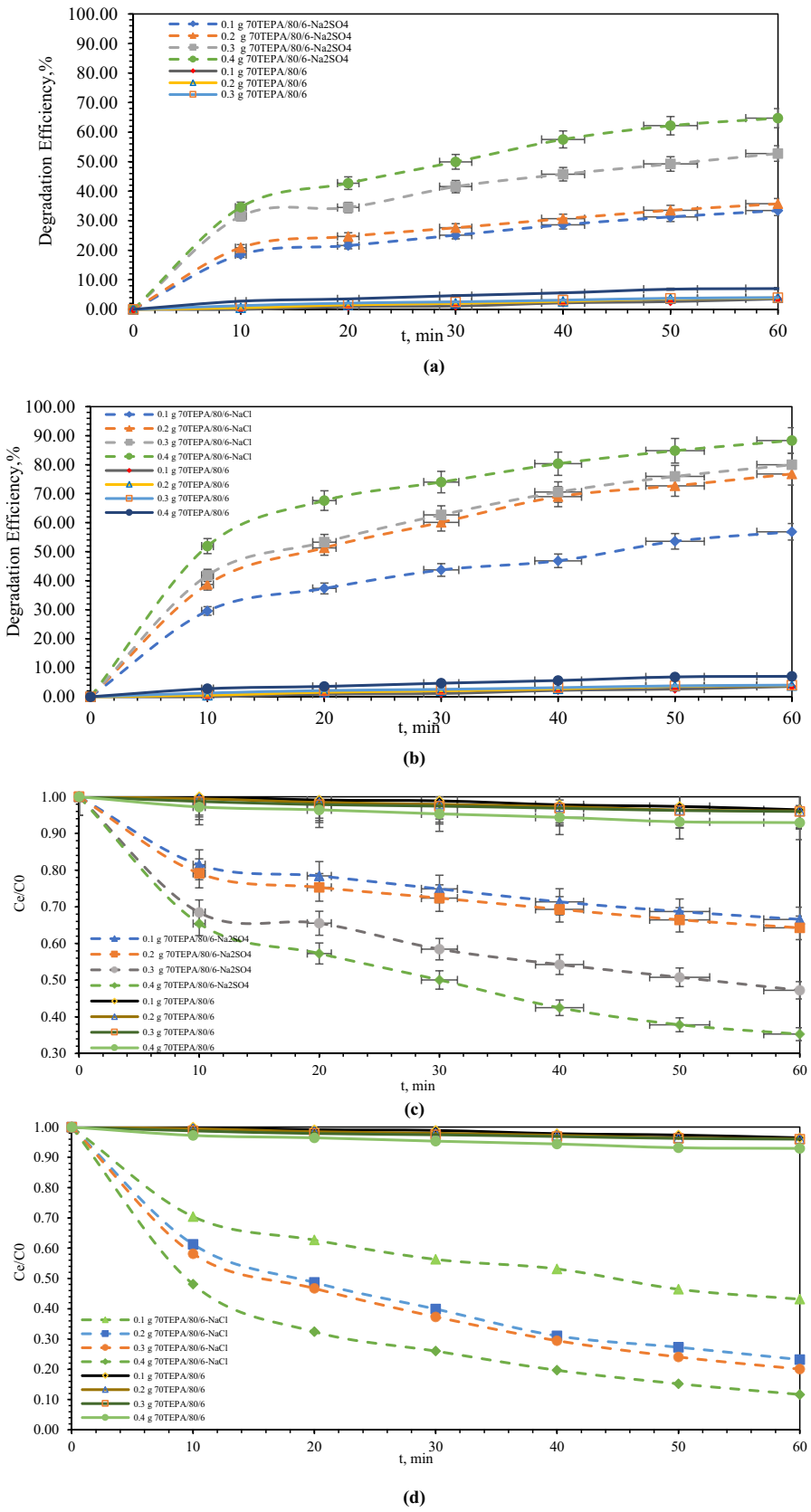

Fig. 9 Effect of particle electrode amount on bentazone degradation efficiency in 3D/EOP. Bentazone degradation efficiency against time for 0.015 M Na_2SO_4 (**a**) and 0.02 M NaCl (**b**). Normalized concentration of bentazone against time for 0.015 M Na_2SO_4 (**c**) and 0.02 M NaCl (**d**)

respectively. Bentazone removal rates of 33.43–64.73% and 56.86–88.3% in Na_2SO_4 and NaCl support electrolytes, respectively, at particle dosages of 2–8 g/L 70TEPA/80/6 in 3D/EOP operating under the same conditions have been obtained (Fig. 9 a and b). As the particle electrodes changed from 2 to 8 g/L, the normalized concentration in the supporting electrolyte Na_2SO_4 decreased from 0.67 to 0.35. In the supporting electrolyte NaCl, the normalized concentration decreased from 0.43 to 0.12 (Fig. 9 c and d).

The oxidation process of pollutants in the three-dimensional electrode system involves direct electron transfer at the anode and the generation of oxidizing species such as H_2O_2, Cl_2, and HClO through electric means (Pulkka et al. 2014). Hydroxyl radicals are believed to be created from water electrolysis in the indirect oxidation process. Activated carbon has been shown in numerous studies to act as a catalyst for breaking down hydrogen peroxide into hydroxyl radicals due to the presence of polyaromatic moieties and functional groups (Lücking et al. 1998; Fortuny et al. 1998; Wu et al. 2005; Navalon et al. 2011). This results in a higher concentration of hydroxyl radicals in the three-dimensional system compared to the two-dimensional system. In the three-dimensional electrode system, activated carbon forms numerous microelectrodes in the electric field, which enhances direct electrochemical oxidation. Particle electrodes in the three-dimensional electrochemical process give it an edge over the traditional two-dimensional electrochemical system.

Charged microparticles designed with TEPA molecules provide a larger surface area than traditional planar electrodes, providing numerous active sites for the electro-oxidation reaction and improving degradation efficiency (Mao et al. 2015; Li et al. 2019). With their increased surface area and porosity, particle electrodes can more effectively facilitate electron transfer reactions, potentially increasing the efficiency of electron transfer during the electro-oxidation process and resulting in faster degradation rates of bentazone (Jung et al. 2015). Li and his team conducted a study to investigate the breakdown of atrazine using a three-dimensional (3D) electrochemical process with $CuFe_2O_4$ as a catalyst. They stated that in the 3D setup, when subjected to an electric field, $CuFe_2O_4$ particles become charged and transform into microcells (Li et al. 2019).

In addition, the electrostatic attraction between the charged particles 70TEPA/80/6 and bentazone caused an increase in the concentration of bentazone molecules at the solution interface with the surface of the particle electrodes. Thus, the increase in particle electrodes allowed the direct oxidation of more bentazone molecules on their surface. (Ahn ve ark. 2009).

Ji et al. studied using Zn-Fe-rich granular sludge carbon to remove bisphenol A (BPA) and Rhodamine B (RhB) in a continuous-flow three-dimensional electrode reactor. They stated that Zn-Fe-rich granular sludge showed low adsorption capacity against BPA for 4 h due to its high specific surface area. They stated that with the application of electrical voltage, the BPA removal efficiency suddenly increased to 89.56% (Ji et al. 2018a).

Possible degradation mechanism

Direct electro-oxidation, also known as anodic oxidation, involves the transfer of electrons directly to the pollutant on the surface of the carbon fibre electrode. Alternatively, it can occur through the formation of hydroxyl radicals [OH*] ($E^\circ = 2.80$ vs SHE) on the anode surface through water oxidation (Vasconcelos et al. 2016; Wu et al. 2016). In Eqs. 13–15, N represents the active points on the surface of the anode.

$$2H_2O + 2e^- \rightarrow H_2 + OH^-(\text{cathode}) \tag{13}$$

$$N + H_2O \rightarrow N\left[OH^*\right] + H^+ + e^-(\text{anode}) \tag{14}$$

$$\text{Bentazone} + N\left[OH^*\right] \rightarrow N + H^+ + e^- + mCO_2 + nH_2O \tag{15}$$

When electrochemically oxidizing with carbon fibre, the strength of the N–OH* interaction relies on the chemical reactivity of the hydroxyl radical intermediate, whether it is absorbed or free. In the presence of hydroxyl radicals, organic pollutants undergo complete mineralization like Eq. 15.

Some electrochemical reactions create active species like active chlorine and ozone during indirect electrochemical oxidation. These species then mediate the oxidation of organic pollutants into CO_2 and H_2O, which depends on the oxidation potential and lifespan of the oxidizing species. Anodic ozone production can occur when the anode's potential exceeds the standard E° potential for ozone formation, 1.8 V, as shown in Eq. 20 (Szpyrkowicz et al. 2005).

$$3H_2O \leftrightarrow O_3 + 6H^+ + 6e^- \tag{16}$$

$$OH^* \rightarrow O^* + H^+ + e^- \tag{17}$$

$$2O^* \rightarrow O_2 \tag{18}$$

$$3H_2O + O_2 \leftrightarrow O_3 + 2H^+ + 2e^- \tag{19}$$

Equation 20 shows that in an acidic solution, molecular oxygen is reduced at the cathode surface, resulting in the continuous production of hydrogen peroxide electrochemically ($E^\circ = 1.8$ V/SHE) (Vasconcelos et al. 2016).

$$O_2 + 2H^+ + 2e^- \rightarrow H_2O_2 \quad E^\circ = 1.8\text{V/SHE} \tag{20}$$

The presence of sulfate in the solution causes the generation of SO_4^{*-} through anodic reaction (Eq. 23). Additionally, the produced SO_4^{*-} reacts with OH^* and H_2O_2 to form HSO_5^- and HO_2^* as Eq. 24 and Eq. 25. It is worth noting that the oxidants produced have weaker oxidation potentials compared to OH^- and H_2O_2 (Cho et al. 2020).

$$SO_4^{*-} + e^- \rightarrow SO_4^{2-} \quad E^\circ = 2.5 - 3.1\text{V} \tag{21}$$

$$S_2O_8^{2-} + 2e^- \rightarrow 2SO_4^{2-} \quad E^\circ = 2.01\text{V/SHE} \tag{22}$$

$$2SO_4^{2-} + \left[OH^*\right] \rightarrow SO_4^{*-} + OH^- \tag{23}$$

$$SO_4^{*-} + \left[OH^*\right] \rightarrow HSO_5^- \tag{24}$$

$$SO_4^{*-} + H_2O_2 \rightarrow SO_4^{2-} + H^+ + HO_2^* \tag{25}$$

During the electrochemical oxidation process, the presence of Cl^- ions in the solution causes the formation of powerful oxidizing species such as chlorine, hypochlorous acid, and hypochlorite ions. Collectively, these ions are known as 'active chlorine' (Wu et al. 2016).

$$N \rightarrow N^{+1} + e \tag{26}$$

$$N^{+1} + CI^- \rightarrow N^{+1}Cl_{(ads)} + e \tag{27}$$

$$N^{+1}Cl_{(ads)} + CI^- \leftrightarrow N + Cl_2 \tag{28}$$

The reactions (Eqs. 26–28) described above result in the formation of chlorine at the electrode. This chlorine can then undergo a dismutation reaction in the solution, producing either HClO or ClO^- depending on the pH level. If the pH is low, HClO and Cl^- are produced as Eq. 30. Conversely, if the pH is high, OCl^- ion is produced as Eq. 31 (Szpyrkowicz et al. 2005). When considering the electro-generation process's oxidative power, factoring in the pH dependence is essential. It is worth noting that the standard reduction potential of $Cl_{2(aq)}$ ($E^\circ = 1.36$ V/SHE) and HClO ($E^\circ = 1.49$ V/SHE) is significantly higher than ClO^- ($E^\circ = 0.89$ V/SHE). This indicates faster organic oxidation can be achieved when mediated by chlorine-active species under acidic pH conditions (Garcia-Segura et al. 2018).

$$2Cl^- \rightarrow Cl_{2(aq)} * + 2e^- \quad E^\circ = 1.36\text{ V/SHE} \tag{29}$$

$$Cl_{2(aq)} + H_2O \leftrightarrow HClO^* + H^+ + Cl^{-*} \quad \begin{matrix} E^\circ = 1.49\text{ V/SHE} \\ \text{(low pH)} \end{matrix} \tag{30}$$

$$HClO \leftrightarrow +H^+ + OCl^{-*} \quad \begin{matrix} E^\circ = 0.89\text{ V/SHE)} \\ \text{(high pH)} \end{matrix} \tag{31}$$

Energy consumption

When evaluating electrochemical processes, degradation efficiency and energy consumption are important factors. Therefore, an economic perspective was taken when analysing the data from the bentazone studies. Figure 10 a–f provide information on the changes in efficiency and energy consumption for 3D/EOP and 2D/EOP, which depend on factors such as voltage, *j*, amount of 70TEPA/80/6, supporting electrolyte concentration, and supporting electrolyte type.

As seen in Fig. 10a–d, depending on the current density and the applied potential difference values, it was determined that 2D/EOP consumes more energy than 3D/EOP and performs low bentazone degradation. The use of 3D/EOP microelectrodes has led to an increase in conductivity within the system. For this reason, less energy consumption occurs in 3D reactors than in 2D reactors.

In a study, Sun et al. used Ti-Sn/c-Al_2O_3 as particle electrodes and investigated the electrocatalytic degradation of chloramphenicol. In their study, they stated that microelectrodes increase the conductivity of the reactor under the electric field. Therefore, high chloramphenicol degradation occurs in 3D reactors with lower energy requirements than 2D reactors (Sun et al. 2017).

When Na_2SO_4 and NaCl were used as electrolytes, the reactors' energy requirements increased with the current density increase and the applied potential difference (Fig. 10a–d). Can and his colleagues' research highlighted that energy usage rises as current density increases in 3D reactors. They linked this to heightened electrode reactions, specifically the formation of O_2 or H_2 on the electrode surface, which occurs as current density increases (Can et al. 2014). When the potential difference between 6 and 7 V was applied, the degradation efficiency was obtained as 73.60% and 78.71% in Na_2SO_4 and 84.66% and 81.66% in NaCl, respectively. At current densities of 7.2 mA and 9.6 mA, degradation efficiency was obtained at 63.13% and 69.77% in Na_2SO_4 and at 87.49% and 91.53% in NaCl, respectively. In addition, for 4, 5, 6, and 7 V, energy consumption was obtained as 2.3, 3.17, 4.96, and 6.72 kWh/m^3 in Na_2SO_4 solution, while it was obtained at 2.4, 3.25, 5.02, and 6.82 kWh/m^3 in NaCl solution. Operating at 6 V and 7.2 mA current densities could be the best values for both types of electrolytes, considering performance efficiency and cost-effectiveness.

For 0.1, 0.2, 0.3, and 0.4 g 70TEPA/80/6 amounts, the degradation efficiency was obtained at 33.43, 35.74, 52.77, and 64.73% in Na_2SO_4 solution and 56.86, 76.80, 79.96,

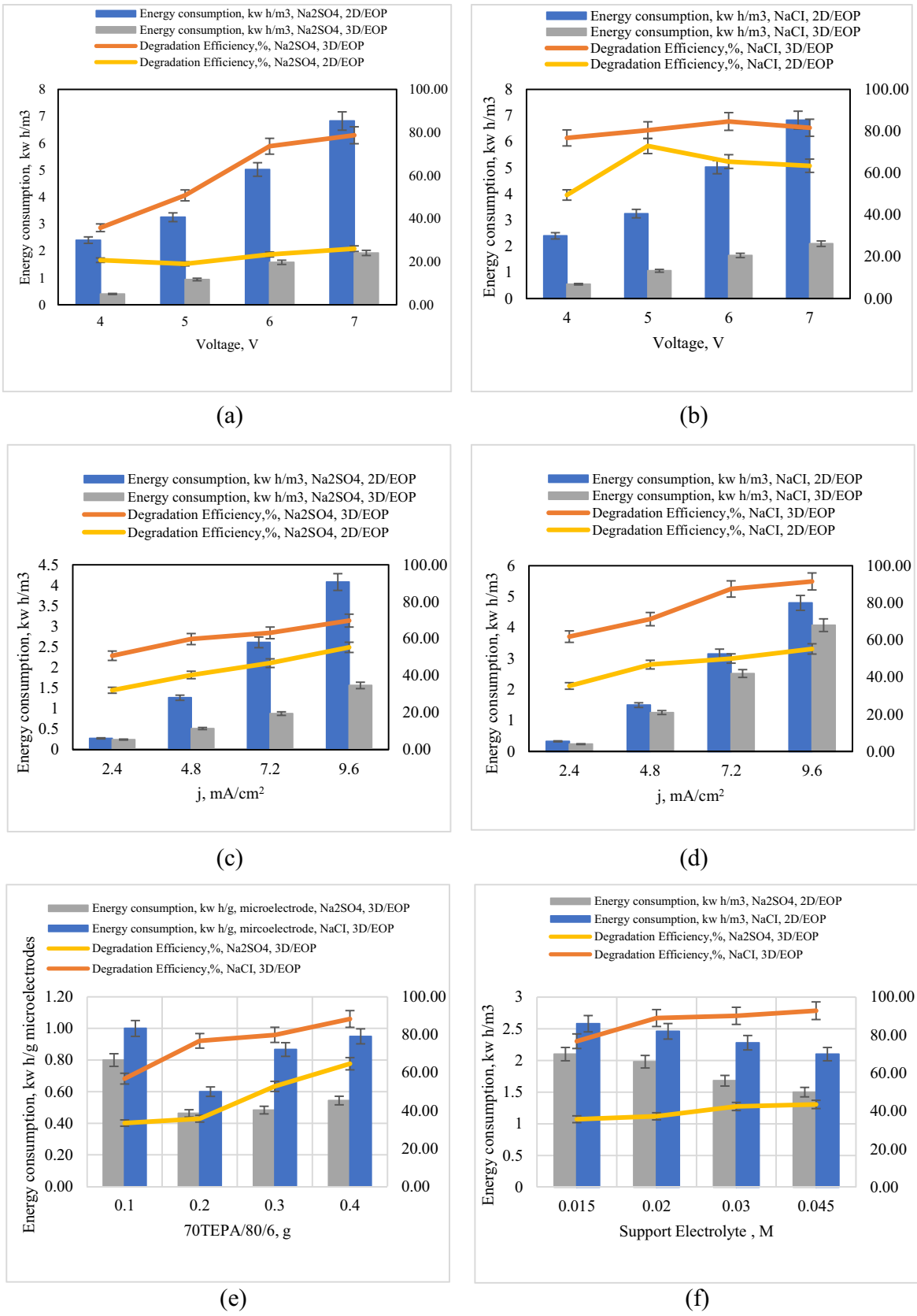

Fig. 10 The energy consumption values and degradation efficiency for 3D/EOP and 2D/EOP reactors

and 88.33% in NaCl solution. In addition, for 0.1, 0.2, 0.3, and 0.4 g 70TEPA/80/6 amounts, energy consumption was obtained at 0.80, 0.46, 0.48, and 0.54 kWh/g microelectrodes in Na_2SO_4 solution, while it was obtained at 1.00, 0.60, 0.87, and 0.95 kWh/g microelectrodes in NaCl solution (Fig. 10e). For bentazone degradation in 3D reactors, considering the energy consumption and efficiency, 0.4 g of 70TEPA/80/6 is suitable when working in Na_2SO_4 solution, while 0.4 g of high energy requirement is required for NaCl solution. For this reason, when NaCl solution is used in bentazone degradation, 0.3 g 70TEPA/80/6 is appropriate.

The energy consumption value decreased when the supporting electrolyte concentration for NaCl and Na_2SO_4 was raised from 0.015 to 0.045 M in the 3D/EOP process (Fig. 10f). This can be explained by the rise in supporting electrolyte concentration and conductivity at a constant current density in the solution, leading to a decrease in potential difference (Cho et al. 2020).

Kinetic study

When using 2D/EOP and 3D/EOP reactors, parameters such as current intensity, electrolyte type, and voltage play an essential role in affecting the degradation kinetics of bentazone in electro-oxidation systems. Experimental results were analysed from a kinetic perspective to understand better the effects of potential difference (voltage, V), current density (j, mA/cm^2), supporting electrolyte concentration (molarity, M), and particle electrode dosage (g) on the bentazone degradation. Different kinetic models were examined by fitting the experimental data using the linearized kinetic models (Eqs. 8–9). The kinetic parameters obtained from the linear fittings (Figures S2–13) are listed in Tables 5 and 6.

The degradation efficiency of bentazone in Na_2SO_4 and NaCl supporting electrolytes was analysed using various parameters. The results showed that the pseudo-first-order kinetic model was more accurate, with a correlation coefficient of 0.997–0.990. During their research on the combined impact of ozone and in situ regenerated granular activated carbon particles in a three-dimensional electrochemical reactor for the effective degradation of nitrobenzene, Wang and his team observed that the degradation of nitrobenzene followed the first-order kinetic model (Wang et al. 2020).

The degradation rate constant k_1 and the heterogeneous rate constant k_h were higher in 3D/EOP than in 2D/EOP. Increasing the voltage from 4 to 7 V had a greater impact on the degradation reaction rate in the 3D/EOP reactor in Na_2SO_4 solution. When the potential difference increased from 4 to 7 V, the $k_{1,3D}$ value in the Na_2SO_4 solution went up by 1.71 times, rising from 0.0042 to 0.0156 min^{-1}.

However, there was not much change in the reaction rate in the 2D/EOP. Voltage level may affect the efficiency and rate of bentazone degradation. Higher voltages can result in increased production of reactive species. In the NaCl solution, the $k_{1,3D}$ value was obtained as 0.0165 for 4 V and 0.0178 for 7 V, and the potential difference did not significantly affect the rate of degradation reaction in 3D/EOP.

Adding particulate electrodes to the degradation process had a notable impact, particularly at a potential difference of 6 V in a Na_2SO_4 solution. At this voltage, the $k_{1,2D}$ value was 0.040×10^{-2} (cm/s) and the heterogeneous rate constant showed 4.5 times increase in 3D/EOP and the $k_{h,3D}$ value was also found to be 0.181×10^{-2} (cm/s).

According to the findings of the experiments investigating the effect of the j (mA/cm^2) value on the reaction rate constant, increasing the j (mA/cm^2) value from 2.4 (mA/cm^2) to 9.6 (mA/cm^2) caused a slight change in the $k_{1,2D}$ value in the Na_2SO_4 solution, but the $k_{1,3D}$ value was 1.5. It was determined that it increased by a factor of 0.011. Increasing the j (mA/cm^2) value to the same levels in the NaCl solution had little effect on the $k_{1.2D}$ value, while the $k_{1.3D}$ value increased by 1.8 times from 0.0108 to 0.0301 min^{-1}. The most significant effect of the change in j (mA/cm^2) value was observed between 2D/EOP and 3D/EOP at 7.2 mA/cm^2 in NaCl solution. While the $k_{1.2D}$ value was measured as 0.0082 min^{-1} at 7.2 mA/cm^2, the reaction rate increased by 2.62 times, and the $k_{1.3D}$ value was obtained as 0.0297 min^{-1}. Increasing the current density increases the production of reactive species such as hydroxyl radicals, which are often responsible for the oxidation of organic compounds such as bentazone. This leads to faster degradation kinetics. However, excessively high current densities may cause side reactions and decreased efficiency.

In the study of the impact of j (mA/cm^2) value and voltage on the reaction rate constant, it was observed that 3D/EOP showed higher k_1 (min^{-1}) values. This indicates that particle electrodes significantly impact increasing the rate of degradation. Using particulate electrodes increases the probability of bentazone molecules encountering OH^- ions formed on the electrode surface while also decreasing the migration distance of bentazone molecules. Furthermore, microelectrodes with TEPA-loaded active points offer a large surface area for direct oxidation to occur. These factors collectively contribute to the increased rate of degradation of bentazone in 3D/EOP.

The degradation rate of bentazone was positively affected by an increase in the amount of particle electrodes in Na_2SO_4 and NaCl solutions. Specifically, when the amount of particle electrode was increased from 0.1 to 0.4 g, the $k_{1,3D}$ value in Na_2SO_4 solution increased by two times from 0.0042 cm^{-1} and reached 0.0128 min^{-1}. Similarly, in the NaCl solution, an increase in the amount of the same particle electrode resulted in the $k_{1,3D}$ value increasing by 1.8 times, reaching a value of 2.83 min^{-1}. These results suggest that an increase in the amount of particle electrode for both

Table 5 First-order kinetic rate constants for electro-oxidative degradation of bentazone in 2D/EOP and 3D/EOP reactors

	Na_2SO_4						NaCl					
	2D/EOP			3D/EOP				2D/EOP			3D/EOP	
	$k_{1,2D}$ (min^{-1})	$k_{h,2D}$ (cm/s)	R^2	$k_{1,3D}$ (min^{-1})	$k_{h,3D}$ (cm/s)	R^2		$k_{1,2D}$ (min^{-1})	$k_{h,2D}$ (cm/s)	R^2	$k_{1,3D}$ (min^{-1})	$k_{h,3D}$ (cm/s)	R^2
Voltage (V)							Voltage (V)						
4	0.0037	4.93E − 4	0.999	0.0042	5.59E − 4	0.999	4	0.0094	1.25E − 4	0.998	0.0165	2.19E − 4	0.999
5	0.0024	3.19E − 4	0.998	0.0072	9.59E − 4	0.998	5	0.0161	2.15E − 4	0.998	0.0186	2.48E − 4	0.993
6	0.0030	3.99E − 4	0.990	0.0136	1.81E − 4	0.999	6	0.0108	1.44E − 4	0.996	0.0196	2.61E − 4	0.990
7	0.0043	5.73E − 4	0.999	0.0156	2.08E − 4	0.993	7	0.0103	1.37E − 4	0.994	0.0178	1.04E − 4	0.984
j (mA/cm^2)							j (mA/cm^2)						
2.4	0.0067	8.93E − 4	0.992	0.0046	6.13E − 4	0.998	2.4	0.0058	7.73E − 4	0.998	0.0108	1.39E − 4	0.998
4.8	0.0091	1.21E − 4	0.989	0.0064	8.53E − 4	0.990	4.8	0.0092	1.23E − 4	0.992	0.016	2.13E − 4	0.999
7.2	0.0074	9.86E − 4	0.989	0.0081	1.08E − 4	0.998	7.2	0.0082	1.09E − 4	0.994	0.0297	3.96E − 4	0.992
9.6	0.0079	1.05E − 4	0.989	0.0110	1.47E − 4	0.998	9.6	0.0087	1.16E − 4	0.999	0.0301	4.01E − 4	0.991
70TEPA/80/6 (g)							70TEPA/80/6 (g)						
0.1				0.0042	5.59E−4	0.993	0.1				0.0097	1.29E−4	0.994
0.2				0.0043	5.73E−4	0.994	0.2				0.0196	2.61E−4	0.997
0.3				0.0077	1.03E−4	0.992	0.3				0.021	2.79E−4	0.992
0.4				0.0128	1.71E−4	0.993	0.4				0.0275	3.67E−4	0.992
Supporting electrolyte (M)							Supporting electrolyte (M)						
0.015				0.0042	5.59E − 4	0.999	0.015				0.0165	2.19E − 4	0.998
0.020				0.0049	6.53E − 4	0.997	0.020				0.0302	4.02E − 4	0.998
0.030				0.0042	5.59E − 4	0.990	0.030				0.0312	4.16E − 4	0.993
0.030				0.0041	5.47E − 4	0.991	0.045				0.0388	5.17E − 4	0.994

Table 6 Second-order kinetic rate constants for electro-oxidative degradation of bentazone in 2D/EOP and 3D/EOP reactors

Na_2SO_4							NaCl					
2D/EOP				3D/EOP			2D/EOP				3D/EOP	
$k_{2,2D}$ (cm^3/mol min)		$k_{h,2D}$ (cm/s)	R^2	$k_{2,3D}$ (cm^3/mol min)	$k_{h,3D}$ (cm/s)	R^2	$k_{2,2D}$ (cm^3/mol min)		$k_{h,2D}$ (cm/s)	R^2	$k_{2,3D}$ (cm^3/mol min)	$k_{h,3D}$ (cm/s)	R^2
Voltage (V)							Voltage (V)						
4	4.21E − 5	5.57E − 5	0.992	0.59E − 4	0.78E − 4	0.991	4	1.49E − 4	1.97E − 04	0.997	4.81E − 4	6.37E − 4	0.997
5	2.78E − 5	3.68E − 5	0.993	1.22E − 4	1.62E − 4	0.996	5	4.15E − 4	5.49E − 04	0.995	6.09E − 4	8.06E − 4	0.981
6	3.67E − 5	4.86E − 5	0.988	3.72E − 4	4.93E − 4	0.989	6	2.46E − 4	3.26E − 04	0.992	8.07E − 4	10.6E − 4	0.981
7	5.24E − 5	6.94E − 5	0.996	4.97E − 4	6.58E − 4	0.965	7	2.24E − 4	2.97E − 04	0.993	6.32E − 4	8.37E − 4	0.979
j (mA/cm^2)							j (mA/cm^2)						
2.4	6.00E − 5	7.9E − 4	0.983	1.16E − 4	15.46E − 4	0.995	2.4	7.81E − 5	10.4E − 4	0.983	1.63E − 5	2.17E − 4	0.993
4.8	9.12E − 5	12.2E − 4	0.976	1.79E − 4	23.86E − 4	0.988	4.8	5.25E − 5	6.9E − 4	0.975	2.88E − 5	3.84E − 4	0.993
7.2	12.4E − 5	16.2E − 4	0.978	1.68E − 4	22.39E − 4	0.994	7.2	13.6E − 5	18.1E − 4	0.991	9.00E − 5	11.9E − 4	0.966
9.6	19.1E − 5	25.5E − 4	0.988	2.14E − 4	28.53E − 4	0.984	9.6	16.0E − 5	21.3E − 4	0.996	1.43E − 5	1.91E − 4	0.962
70TEPA/80/6 (g)							70TEPA/80/6 (g)						
0.1				7.14E − 6	9.52E − 5	0.981	0.1				1.79E − 4	2.39E − 3	0.990
0.2				7.04E − 6	9.38E − 5	0.985	0.2				5.41E − 4	7.21E − 3	0.993
0.3				5.76E − 6	7.68E − 5	0.983	0.3				6.60E − 4	8.79E − 3	0.986
0.4				10.2E − 5	1.36E − 4	0.981	0.4				1.26E − 3	16.79E − 3	0.971
Supporting electrolyte (M)							Supporting electrolyte (M)						
0.015				5.86E − 5	7.81E − 4	0.996	0.015				4.80E − 6	6.39E − 5	0.994
0.020				6.95E − 5	9.26E − 4	0.992	0.020				1.40E − 3	1.87E − 2	0.956
0.030				6.71E − 5	8.94E − 4	0.984	0.030				1.60E − 3	2.13E − 2	0.944
0.030				6.54E − 5	8.72E − 4	0.990	0.045				2.40E − 3	3.19E − 2	0.967

electrolyte solutions improves the degradation efficiency of bentazone.

According to Table 5, increasing the concentration of chloride-supported electrolytes positively impacted bentazone dissociation kinetics. The electrolyte concentration in the solution affects its conductivity. This affects electron transfer rates and degradation kinetics.

However, varying the concentration of sulfate-supported electrolyte did not affect the kinetic results. Murugananthan et al. reported similar results in their study (Murugananthan et al. 2008). It is possible that the reason why the k value remained almost constant at 0.0042 with the change in sulfate concentration is that higher sulfate levels may lead to faster consumption of reactive oxygen species like OH^- and H_2O_2 (Cho et al. 2020).

When the concentration of Cl^- ions in the solution was increased, the bentazone degradation rate rose from 0.0165 to 0.0388 min^{-1}. This was because more reactive chlorine species were produced due to the higher concentration of Cl^- ions in the solution (Wu et al. 2016).

ANN modelling

ANN approach was used to model and predict the effects of input variables (applied potential difference, current density, particle electrode amount, pH, and supporting electrolyte concentration) on output (bentazone degradation). The experimental variables and their ranges are reported in Table 7. The mean square error and the error function were calculated by using Eqs. 11 and 12. To determine the optimum number of the neurons in the hidden layers, the procedure described by Vianayagam et al. (2022) and Sridevi et al. (2023) was followed, in which the range of hidden neurons varied from 1 to 30. Trial and error–based simulation runs to find the optimum number of neurons in the hidden layer indicated that 16, 22, 18, and 15 neurons in the network's hidden layer resulted in the lowest MSE and the high correlation coefficients for bentazone degradation in the 2D and 3D reactors for sodium sulfate and sodium chloride electrolytes. Figure 11 depicts the relation between the ANN network and the number of neurons in the hidden layers.

A five-layered feed-forward back propagation network with 5:16:1, 5:22:1, 5:18:1, and 5:15:1 topology was employed to model the degradation efficiency of bentazone. As observed from Fig. 12a–d, most of the predicted values cluster on the diagonal, resulting in a higher R^2 of ranging from 0.98055 to 0.99937, 0.97096 to 0.99882, 0.96416 to 0.98940, and 0.97953 to 0.99649 for the training, validation, test, and all of the bentazone degradation in reactors above and electrolytes. It is evident from the ANN modelling results that the selected neural network architecture successfully exhibits strong linearity with the target values. The overall performances of the artificial neural network for 2D and 3D electro-oxidation reactors and the electrolytes, Na_2SO_4 and NaCl, are depicted in Figures S14–17.

The sensitivity analysis was employed to determine the relative importance of the four and five inputs in the 2D

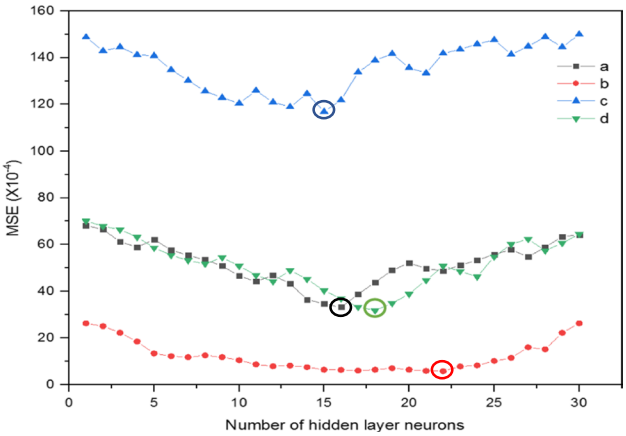

Fig. 11 Selection of the best ANN architecture based on the lowest MSE values of trained ANN topologies Na_2SO_4 electrolyte in the 2D reactor (a), NaCl electrolyte in the 2D reactor (b), Na_2SO_4 electrolyte in the 3D reactor (c), and NaCl electrolyte in the 3D reactor (d)

Table 7 Input variables, their ranges, and relative importance of experimental variables on the degradation efficiency (%) of bentazone

			Input variables					Output variable
		Topology	Voltage (V)	Current density (mA/cm^2)	Particle electrode amount (g)	Supporting electrolyte concentration (M)	pH	Degradation efficiency (%)
Range			4–7	2.4–9.6	0.1–0.4	0.015–0.045	3–9	100
Reactor	Electrolyte		Relative importance (%)					
2D	Na_2SO_4	4:16:1	41.84	46.21	-	6.52	5.43	
2D	NaCl	4:22:1	40.70	48.22	-	6.11	4.97	
3D	Na_2SO_4	5:15:1	33.22	19.42	28.11	10.43	8.82	
3D	NaCl	5:18:1	32.09	20.25	29.75	9.86	8.05	

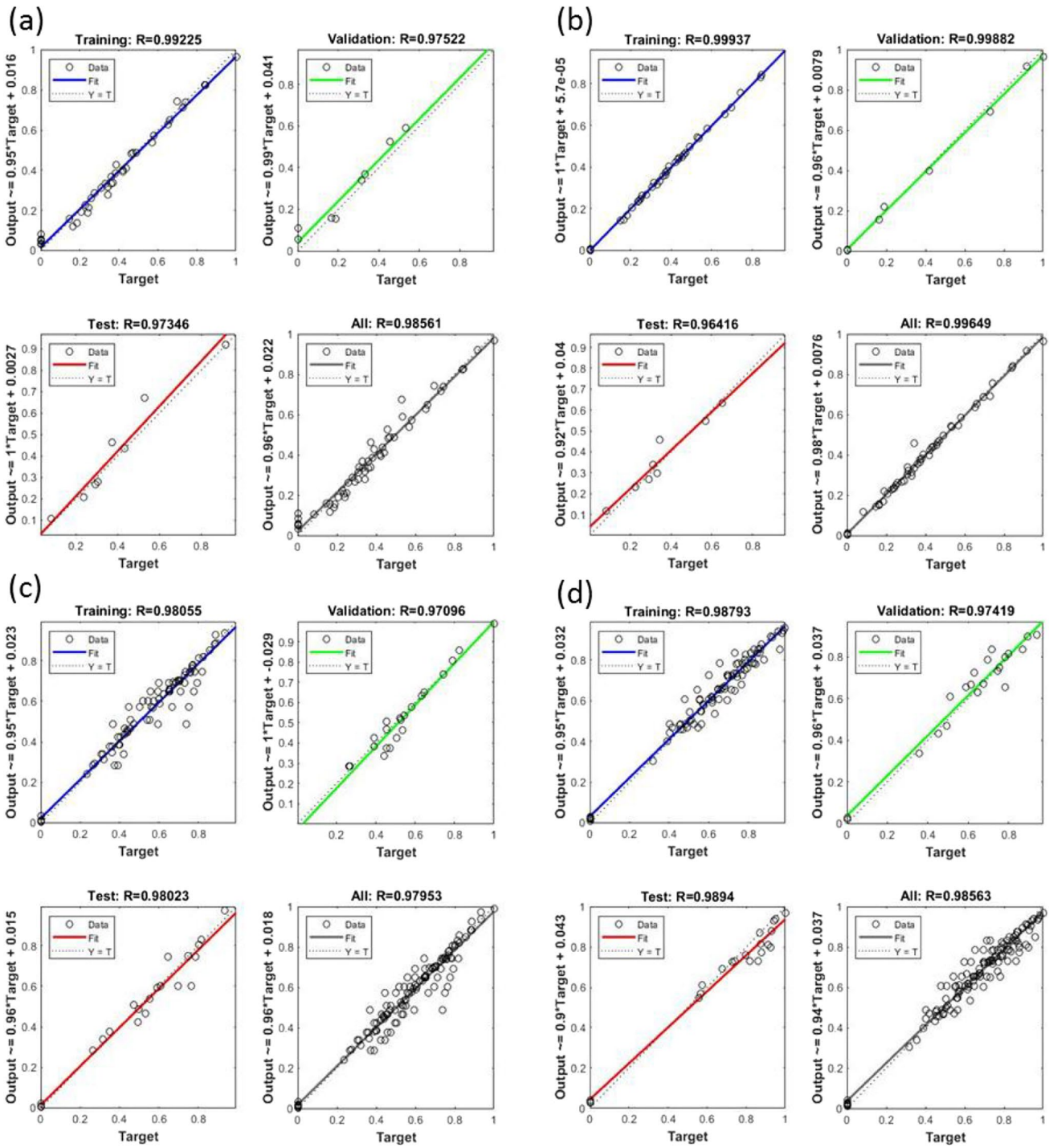

Fig. 12 Regression plots during ANN modelling of bentazone degradation for Na_2SO_4 electrolyte in 2D reactor (**a**), NaCl electrolyte in 2D reactor (**b**), Na_2SO_4 electrolyte in 3D reactor (**c**), and NaCl electrolyte in 3D reactor (**d**)

and 3D electro-oxidation reactors on bentazone degradation. It is clear from Table 7 that the current density and voltage for each electrolyte had the most significant impact on the 2D reactors. The pH and electrolyte concentration demonstrated far less importance. In the case of the 3D electro-oxidation reactors, on the other hand, the voltage and particle electrode amount for the electrolytes had considerable importance on the bentazone degradation. The current density assumed moderate importance, accounting for 19.42% and 20.25% for Na_2SO_4 and NaCl electrolytes, respectively. The pH and supporting electrolyte concentration, similar to those of the 2D electro-oxidation reactor,

exhibited minor importance among the bentazone degradation parameters.

Synergistic effect

When TEPA-loaded particles come into contact with bentazone molecules, bentazone can be adsorbed on the TEPA surface. Figure 13 a and b display the synergistic effects at 4V to illustrate how adsorption affects the 3D electrooxidation process and highlights the combined effect. The synergistic effect was evaluated using the synergistic factor S_f (Eq. 2). According to Fig. 13a, b, the synergistic factors (S_f) remained above 0 for the entire 60 min duration when the potential difference of 4 V was applied to Na_2SO_4 and NaCl solution. This indicates that the degradation efficiency of 3D/EOP is superior to the combined efficiency of 2D/EOP and adsorption on their own (Fig. 14). In a Na_2SO_4 solution, the S_f value was notably high when 0.3 and 0.4 g of 70TEPA/80/6 were utilized. This effect was observed when dosages of 0.2, 0.3, and 0.4 g of 70TEPA/80/6 were used in a NaCl solution. This occurrence is due to the inefficiency of the adsorption mechanism during the process. These results show that 70TEPA/80/6 microelectrodes, which become charged particles under the electric field, significantly contribute to the degradation of bentazone.

Conclusion

The study aimed to examine how particle electrodes affect the efficiency of carbon fibre electrodes in degrading bentazone within a three-phase, three-dimensional electrochemical system. Specifically, activated carbons were utilized as particle electrodes, enriched with TEPA molecules to ensure a three-phase and three-dimensional system. Below are the significant findings from this study:

This study investigated the performance of 2D and 3D electrooxidation systems for the effective degradation of bentazone, an herbicide commonly used in agriculture and moderately harmful to humans, and the implications of several variables that may influence this performance. It was demonstrated that 3D/EOP, which used TEPA-modified activated carbons as particle electrodes for bentazone removal, performed much better than 2D/EOP. The highest degradation efficiency, 91.53%, was achieved in the 3D/EOP, with an energy consumption of 4.8 kWh/m^3. The 2D/EOP achieved a maximum degradation efficiency of 55.88%, with an energy consumption of 4.08 kWh/m^3. The first-order kinetic model indicates that the highest rate of bentazone degradation was 0.0092 1/min with 2D/EOP, while the rate reached 0.0388 1/min with 3D/EOP. These results were obtained when sodium chloride was used as the supporting electrolyte. Considering the balance between energy consumption and distortion efficiency, 3D/EOP systems seem preferable in practice. The data obtained from the experiments were analysed with an artificial neural network (ANN) to ensure the reliability of the results. Coefficients of determination (R^2) were high values ranging from 0.97953 to 0.99649. A sensitivity analysis was used to determine the relative effect of experimental parameters on bentazone degradation. In 2D reactors, current density and voltage are the most critical parameters for each electrolyte. However, in 3D reactors, voltage and particle electrode amount are also important parameters. These findings indicate that 3D electrochemical oxidation systems with TEPA-modified particle electrodes are a suitable alternative for the high-level degradation of organic pollutants such as bentazone. Also, 3D/EOP with TEPA microelectrode content has the potential to be applied to the real world. Nanostructured or composite microelectrodes can be used to improve the adsorption and degradation of bentazone molecules. To synergistically increase bentazone degradation, electrochemical methods can be combined with other advanced treatment processes such as ozonation or UV irradiation, and plot studies can be performed.

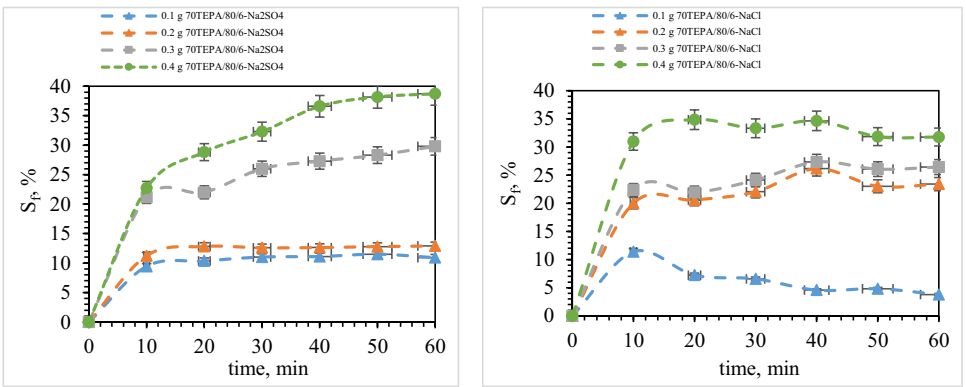

Fig. 13 Synergistic factors vs. time with different amount of 70TEPA/80/6 in Na_2SO_4 (**a**), and NaCl (**b**)

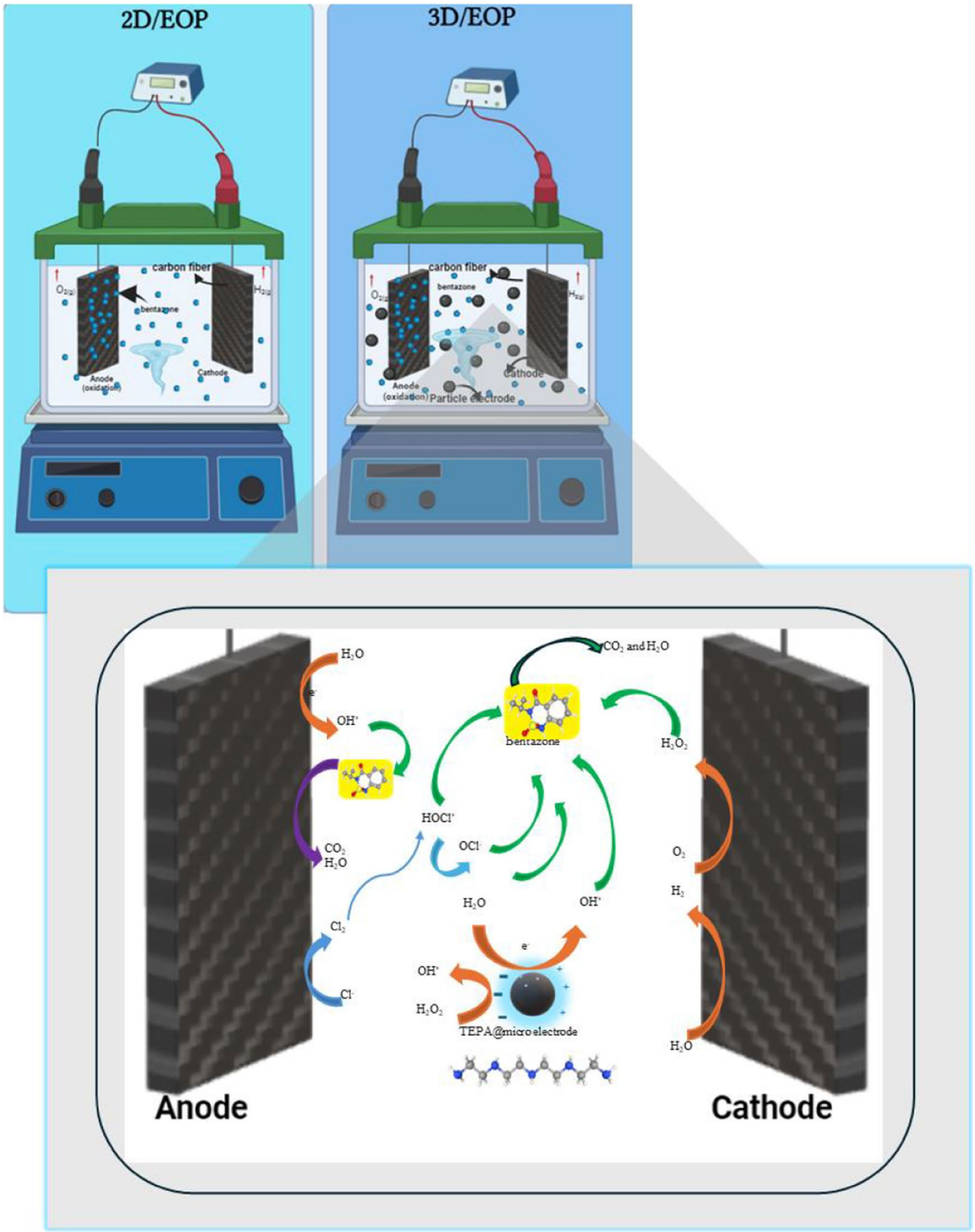

Fig. 14 Schematic view of reactors (2D/EOP and 3D/EOP) and degradation mechanism of bentazone in 3D/EOP

Acknowledgements We would like to express our gratitude to Tugce Bozkurt and Hatice Hürrem Cin for their valuable contributions to the study.

Author contribution Canan Samdan: conceptualization, methodology, validation, analysis, investigation, writing, original draft, project management. Hakan Demiral: conceptualization, methodology, formal analysis, writing, review, editing. Yunus Emre Simsek: conceptualization, methodology, data curation and analysis, writing, review. Ilknur Demiral: writing, review, editing, supervision. Belgin Karabacakoglu: conceptualization, methodology, writing, review, editing, supervision. Tugce Bozkurt: conceptualization, methodology. Hatice Hürrem Cin: conceptualization, methodology.

Funding The author declares that this study has been funded by the Scientific Research Foundation, Eskisehir Osmangazi University under grant numbers FBA-2021–1591.

Data availability Not applicable.

Declarations

Ethics approval All ethical rules have been read and applied as written.

Consent to participate The study does not contain any information that would require consent from any individual.

Consent for publication The study is not a case study. It does not contain information that would require an individual's consent.

Competing interests The authors declare no competing interests.

References

Abd El-Magied MO, Hassan AMA, Gad HMH et al (2018) Removal of nickel (II) ions from aqueous solutions using modified activated carbon: a kinetic and equilibrium study. J Dispersion Sci Technol 39:862–873. https://doi.org/10.1080/01932691.2017.1402337

Abdulaal AH, Valizadeh M, Amirani MC, Shahen Shah AFM (2024) A self-learning deep neural network for classification of breast histopathological images. Biomed Signal Process Control 87:105418. https://doi.org/10.1016/j.bspc.2023.105418

Ahmad M, Liu S, Mahmood N et al (2017) Effects of porous carrier size on biofilm development, microbial distribution and nitrogen removal in microaerobic bioreactors. Biores Technol 234:360–369. https://doi.org/10.1016/j.biortech.2017.03.076

Ahmad M, Yousaf M, Han J-C et al (2023) State-of-the-art analysis of the fuel desulphurization processes: perspective of CO2 utilization in coal biodesulphurization. Chem Eng J 478:147517. https://doi.org/10.1016/j.cej.2023.147517

Ahmad Isiyaka H, Jumbri K, Soraya Sambudi N et al (2022) Effective adsorption of metolachlor herbicide by MIL-53(Al) metal-organic framework: optimization, validation and molecular docking simulation studies. Environ Nanotechnol, Monit Manag 18:100663. https://doi.org/10.1016/j.enmm.2022.100663

Ahmadian Hosseini A, Jahandar Lashaki M (2023) A comprehensive evaluation of amine-impregnated silica materials for direct air capture of carbon dioxide. Sep Purif Technol 325:124580. https://doi.org/10.1016/j.seppur.2023.124580

Ahn CK, Park D, Woo SH, Park JM (2009) Removal of cationic heavy metal from aqueous solution by activated carbon impregnated with anionic surfactants. J Hazard Mater 164:1130–1136. https://doi.org/10.1016/j.jhazmat.2008.09.036

Akram M, Rani M, Batool K et al (2024) Lead integrated two-dimensional (MXene/PbCrO 4) nanocomposite designed for energy storage and photocatalytic degradation applications. Phys Scr 99:015902. https://doi.org/10.1088/1402-4896/ad0fcd

Al-Laham M, Kassaymeh S, Al-Betar MA et al (2023) An efficient convergence-boosted salp swarm optimizer-based artificial neural network for the development of software fault prediction models. Comput Electr Eng 111:108923. https://doi.org/10.1016/j.compeleceng.2023.108923

Ancy K, Vijilvani C, Bindhu MR et al (2021) Visible light assisted photocatalytic degradation of commercial dyes and waste water by Sn–F co-doped titanium dioxide nanoparticles with potential antimicrobial application. Chemosphere 277:130247. https://doi.org/10.1016/j.chemosphere.2021.130247

Arjona N, Guerra-Balcázar M, Álvarez-Contreras L (2022) Hierarchical Pd and Pt structures obtained on 3D carbon electrodes as electrocatalysts for the ethylene glycol electro-oxidation. Appl Surf Sci 571:151246. https://doi.org/10.1016/j.apsusc.2021.151246

Azpiri Solares RA, Soares dos Santos D, Ingram A, Wood J (2019) Modelling and parameter estimation of breakthrough curves for amine-modified activated carbons under pre-combustion carbon capture conditions. Fuel 253:1130–1139. https://doi.org/10.1016/j.fuel.2019.05.095

Basir S, Senocak I (2022) Physics and equality constrained artificial neural networks: application to forward and inverse problems with multi-fidelity data fusion. J Comput Phys 463:111301. https://doi.org/10.1016/j.jcp.2022.111301

Cai N, Bai G, Zhang T, et al (2023) Three-dimensional heterogeneous electro-Fenton system with reduced graphene oxide based particle electrode for Acyclovir removal. Chin Chem Lett 108514. https://doi.org/10.1016/j.cclet.2023.108514

Can W, Yao-Kun H, Qing Z, Min J (2014) Treatment of secondary effluent using a three-dimensional electrode system: COD removal, biotoxicity assessment, and disinfection effects. Chem Eng J 243:1–6. https://doi.org/10.1016/j.cej.2013.12.044

Cao H (2023) TEPA-SiO2@PDA composite as a highly stable underwater oleophobic coating on copper mesh for oil-water separation with high flux. Prog Org Coat 177:107446. https://doi.org/10.1016/j.porgcoat.2023.107446

Carvalho JA, Gaiotti AC, Zanata CR et al (2023) How does CO co-adsorption affect glycerol electro-oxidation on polycrystalline platinum? In situ FTIR and DFT approaches. Electrochim Acta 443:141978. https://doi.org/10.1016/j.electacta.2023.141978

Cerejeira MJ, Viana P, Batista S et al (2003) Pesticides in Portuguese surface and ground waters. Water Res 37:1055–1063. https://doi.org/10.1016/S0043-1354(01)00462-6

Chen H, Feng Y, Suo N et al (2019) Preparation of particle electrodes from manganese slag and its degradation performance for salicylic acid in the three-dimensional electrode reactor (TDE). Chemosphere 216:281–288. https://doi.org/10.1016/j.chemosphere.2018.10.097

Cheng S, Pang X, Jiang G, Pang J (2024) Epoxy lignin-modified tetraethylenepentamethylene-CO2 halogen-free blown rigid polyurethane foam. Constr Build Mater 414:134929. https://doi.org/10.1016/j.conbuildmat.2024.134929

Cho S, Kim C, Hwang I (2020) Electrochemical degradation of ibuprofen using an activated-carbon-based continuous-flow three-dimensional electrode reactor (3DER). Chemosphere 259:127382. https://doi.org/10.1016/j.chemosphere.2020.127382

Deng H, Yang L, Tao G, Dai J (2009) Preparation and characterization of activated carbon from cotton stalk by microwave assisted chemical activation—application in methylene blue adsorption from aqueous solution. J Hazard Mater 166:1514–1521. https://doi.org/10.1016/j.jhazmat.2008.12.080

Deng Y, Zhu X, Chen N et al (2020) Review on electrochemical system for landfill leachate treatment: performance, mechanism, application, shortcoming, and improvement scheme. Sci Total Environ 745:140768. https://doi.org/10.1016/j.scitotenv.2020.140768

Dinda S (2023) In-situ grafted amine functionalized metal-organic frameworks for CO2 capture: preparation and bench-scale performance evaluation. Mater Today Commun 35:105927. https://doi.org/10.1016/j.mtcomm.2023.105927

FAO (2022) Pesticides use, pesticides trade and pesticides indicators. FAO

FAO/WHO (2016) Pesticide residues in food 2016: Joint FAO/WHO meeting on pesticide residues: report of the joint meeting of the FAO panel of experts on pesticide residues in food and the environment and the WHO core assessment group on pesticide residues: Rome, Italy, 13–22 September 2016. World Health Organization: Food Agric Org United Nations, Rome

FAOSTAT (2023) FAOSTAT. https://www.fao.org/faostat/en/#data/RP. Accessed 8 Jul 2023

Foroughi M, Rahmani AR, Asgari G et al (2020) Optimization and modeling of tetracycline removal from wastewater by three-dimensional electrochemical system: application of response surface methodology and least squares support vector machine. Environ Model Assess 25:327–341. https://doi.org/10.1007/s10666-019-09675-9

Fortuny A, Font J, Fabregat A (1998) Wet air oxidation of phenol using active carbon as catalyst. Appl Catal B 19:165–173. https://doi.org/10.1016/S0926-3373(98)00072-1

Garcia-Segura S, Ocon JD, Chong MN (2018) Electrochemical oxidation remediation of real wastewater effluents — a review. Process Saf Environ Prot 113:48–67. https://doi.org/10.1016/j.psep.2017.09.014

Garson GD (1991) Interpreting neural-network connection weights. AI Expert (6):47–51

Gaynor JD, MacTavish DC (1981) Pentafluorobenzyl, (trifluoromethyl)benzyl and diazomethane alkylation of bentazon for residue determination in soil by gas chromatography. J Agric Food Chem 29:626–629. https://doi.org/10.1021/jf00105a047

Ghattas B, Manzon D (2023) Machine learning alternatives to response surface models. Mathematics 11:3406. https://doi.org/10.3390/math11153406

Ghorbani F, Kamari S, Zamani S et al (2020) Optimization and modeling of aqueous Cr(VI) adsorption onto activated carbon prepared from sugar beet bagasse agricultural waste by application of response surface methodology. Surf Interfaces 18:100444. https://doi.org/10.1016/j.surfin.2020.100444

Gineys M, Benoit R, Cohaut N et al (2017) Behavior of activated carbon cloths used as electrode in electrochemical processes. Chem Eng J 310:1–12. https://doi.org/10.1016/j.cej.2016.10.018

Gottipati R, Mishra S (2016) Preparation of microporous activated carbon from Aegle marmelos fruit shell and its application in removal of chromium(VI) from aqueous phase. J Ind Eng Chem 36:355–363. https://doi.org/10.1016/j.jiec.2016.03.005

Guo Y, Rockstraw DA (2007) Activated carbons prepared from rice hull by one-step phosphoric acid activation. Microporous Mesoporous Mater 100:12–19. https://doi.org/10.1016/j.micromeso.2006.10.006

Guo M, Xiong J, Jin X et al (2023) Mussel stimulated modification of flexible Janus PAN/PVDF-HFP nanofiber hybrid membrane for advanced lithium-ion batteries separator. J Membr Sci 675:121533. https://doi.org/10.1016/j.memsci.2023.121533

Hajiahmadi M, Zarei M, Khataee A (2022) An effective natural mineral-catalyzed heterogeneous electro-Fenton method for degradation of an antineoplastic drug: modeling by a neural network. Chemosphere 291:132810. https://doi.org/10.1016/j.chemosphere.2021.132810

Han J-C, Ahmad M, Yousaf M et al (2023) Strategic analysis on development of simultaneous adsorption and catalytic biodegradation over advanced bio-carriers for zero-liquid discharge of industrial wastewater. Chemosphere 332:138871. https://doi.org/10.1016/j.chemosphere.2023.138871

He W, Ma Q, Wang J et al (2014) Preparation of novel kaolin-based particle electrodes for treating methyl orange wastewater. Appl Clay Sci 99:178–186. https://doi.org/10.1016/j.clay.2014.06.030

Hu C, Liu F, Lan H et al (2015) Preparation of a manganese dioxide/carbon fiber electrode for electrosorptive removal of copper ions from water. J Colloid Interface Sci 446:359–365. https://doi.org/10.1016/j.jcis.2014.12.051

Hu Z, Wang J, Sun T (2024) Tetraethylenepentamine-functionalized magnetic mesoporous composites as a novel adsorbent for the removal Cr(III)-ethylenediaminetetraacetic acid in complex solution. Chin J Chem Eng 68:16–26. https://doi.org/10.1016/j.cjche.2024.01.004

Huang X-Y, Mao X-Y, Bu H-T et al (2011) Chemical modification of chitosan by tetraethylenepentamine and adsorption study for anionic dye removal. Carbohyd Res 346:1232–1240. https://doi.org/10.1016/j.carres.2011.04.012

Huang P, Wei X, Wang X et al (2023) Facile fabrication of silica aerogel supported amine adsorbent pellets for Low-concentration CO2 removal from confined spaces. Chem Eng J 468:143629. https://doi.org/10.1016/j.cej.2023.143629

Isarain-Chávez E, Baró MD, Rossinyol E et al (2017) Comparative electrochemical oxidation of methyl orange azo dye using Ti/Ir-Pb, Ti/Ir-Sn, Ti/Ru-Pb, Ti/Pt-Pd and Ti/RuO 2 anodes. Electrochim Acta 244:199–208. https://doi.org/10.1016/j.electacta.2017.05.101

Ji J, Li X, Xu J et al (2018a) Zn-Fe-rich granular sludge carbon (GSC) for enhanced electrocatalytic removal of bisphenol A (BPA) and Rhodamine B (RhB) in a continuous-flow three-dimensional electrode reactor (3DER). Electrochim Acta 284:587–596. https://doi.org/10.1016/j.electacta.2018.07.203

Ji J, Liu Y, Yang X et al (2018b) Multiple response optimization for high efficiency energy saving treatment of rhodamine B wastewater in a three-dimensional electrochemical reactor. J Environ Manage 218:300–308. https://doi.org/10.1016/j.jenvman.2018.04.071

Jiang G-B, Lin Z-T, Huang X-Y et al (2012) Potential biosorbent based on sugarcane bagasse modified with tetraethylenepentamine for removal of eosin Y. Int J Biol Macromol 50:707–712. https://doi.org/10.1016/j.ijbiomac.2011.12.030

Jing M, Jiang L, Yi B, Sun G (2013) Comparative study of methanol adsorption and electro-oxidation on carbon-supported platinum in acidic and alkaline electrolytes. J Electroanal Chem 688:172–179. https://doi.org/10.1016/j.jelechem.2012.10.028

Joudi NAE, Othmani MB, Bourzgui F et al (2022) Review of the role of artificial ıntelligence in dentistry: current applications and trends. Procedia Comp Sci 210:173–180. https://doi.org/10.1016/j.procs.2022.10.134

Jung K-W, Hwang M-J, Park D-S, Ahn K-H (2015) Performance evaluation and optimization of a fluidized three-dimensional electrode reactor combining pre-exposed granular activated carbon as a moving particle electrode for greywater treatment. Sep Purif Technol 156:414–423. https://doi.org/10.1016/j.seppur.2015.10.030

Khelifa A, Moulay S, Naceur AW (2005) Treatment of metal finishing effluents by the electroflotation technique. Desalination 181:27–33. https://doi.org/10.1016/j.desal.2005.01.011

Khoshraftar Z, Taheri FS, Nezami S, Ghaemi A (2023) Using halloysite nanotubes modified by tetraethylenepentamine for advanced carbon capture: experimental and modeling via RSM and ANNs. Chem Eng J Adv 16:100543. https://doi.org/10.1016/j.ceja.2023.100543

Kong Y, Chen X, Ni J et al (2010) Palygorskite–expanded graphite electrodes for catalytic electro-oxidation of phenol. Appl Clay Sci 49:64–68. https://doi.org/10.1016/j.clay.2010.04.003

Konya A, Nematzadeh P (2024) Recent applications of AI to environmental disciplines: a review. Sci Total Environ 906:167705. https://doi.org/10.1016/j.scitotenv.2023.167705

Kumar PS, Raja MJS, Kumaresan M et al (2014) A new electrode reactor with in-built recirculation mode for the enhancement of methylene blue dye removal from the aqueous solution: comparison of adsorption, electrolysis and combined effect. Korean J Chem Eng 31:276–283. https://doi.org/10.1007/s11814-013-0209-2

Kumar S, Singh S, Srivastava VC (2015) Electro-oxidation of nitrophenol by ruthenium oxide coated titanium electrode: parametric, kinetic and mechanistic study. Chem Eng J 263:135–143. https://doi.org/10.1016/j.cej.2014.11.051

Li M, Zhao F, Sillanpää M et al (2015) Electrochemical degradation of 2-diethylamino-6-methyl-4-hydroxypyrimidine using three-dimensional electrodes reactor with ceramic particle electrodes. Sep Purif Technol 156:588–595. https://doi.org/10.1016/j.seppur.2015.10.053

Li J, Yan J, Yao G et al (2019) Improving the degradation of atrazine in the three-dimensional (3D) electrochemical process using CuFe2O4 as both particle electrode and catalyst for persulfate activation. Chem Eng J 361:1317–1332. https://doi.org/10.1016/j.cej.2018.12.144

Liou T-H (2010) Development of mesoporous structure and high adsorption capacity of biomass-based activated carbon by phosphoric acid and zinc chloride activation. Chem Eng J 158:129–142. https://doi.org/10.1016/j.cej.2009.12.016

Liu X, Zhang Y (2024) Nitrogen-doped reduced graphene oxide (N-rGO) three-dimensional electrode electrochemically activates persulfate for the degradation of tetracycline. Carbon Lett 34:865–879. https://doi.org/10.1007/s42823-024-00701-9

Liu S-H, Hsiao W-C, Sie W-H (2012) Tetraethylenepentamine-modified mesoporous adsorbents for CO2 capture: effects of preparation methods. Adsorption 18:431–437. https://doi.org/10.1007/s10450-012-9429-8

Liu Z, Zhao C, Wang P et al (2018) Removal of carbamazepine in water by electro-activated carbon fiber-peroxydisulfate: comparison, optimization, recycle, and mechanism study. Chem Eng J 343:28–36. https://doi.org/10.1016/j.cej.2018.02.114

Liu Y-J, Hu C-Y, Lo S-L (2019) Direct and indirect electrochemical oxidation of amine-containing pharmaceuticals using graphite electrodes. J Hazard Mater 366:592–605. https://doi.org/10.1016/j.jhazmat.2018.12.037

Liu Y, Sun T, Su Q et al (2020) Highly efficient and mild electrochemical degradation of bentazon by nano-diamond doped PbO2 anode with reduced Ti nanotube as the interlayer. J Colloid Interface Sci 575:254–264. https://doi.org/10.1016/j.jcis.2020.04.092

Liu Y, Jin J, Zhao H (2024) Deep learning-based pulsar candidate identification model using a variational autoencoder. New Astron 106:102125. https://doi.org/10.1016/j.newast.2023.102125

Lücking F, Köser H, Jank M, Ritter A (1998) Iron powder, graphite and activated carbon as catalysts for the oxidation of 4-chlorophenol with hydrogen peroxide in aqueous solution. Water Res 32:2607–2614. https://doi.org/10.1016/S0043-1354(98)00016-5

Malla MA, Dubey A, Kumar A et al (2023) Modeling and optimization of chlorpyrifos and glyphosate biodegradation using RSM and ANN: elucidating their degradation pathways by GC-MS based metabolomics. Ecotoxicol Environ Saf 252:114628. https://doi.org/10.1016/j.ecoenv.2023.114628

Mao R, Zhao X, Lan H et al (2015) Graphene-modified Pd/C cathode and Pd/GAC particles for enhanced electrocatalytic removal of bromate in a continuous three-dimensional electrochemical reactor. Water Res 77:1–12. https://doi.org/10.1016/j.watres.2015.03.002

Martínez-Huitle CA, Brillas E (2009) Decontamination of wastewaters containing synthetic organic dyes by electrochemical methods: a general review. Appl Catal B 87:105–145. https://doi.org/10.1016/j.apcatb.2008.09.017

Meng H, Chen C, Yan Z et al (2019) Co-doping polymethyl methacrylate and copper tailings to improve the performances of sludge-derived particle electrode. Water Res 165:115016. https://doi.org/10.1016/j.watres.2019.115016

Momcilovic M, Purenovic M, Bojic A et al (2011) Removal of lead(II) ions from aqueous solutions by adsorption onto pine cone activated carbon. Desalination 276:53–59. https://doi.org/10.1016/j.desal.2011.03.013

Murugananthan M, Yoshihara S, Rakuma T, Shirakashi T (2008) Mineralization of bisphenol A (BPA) by anodic oxidation with boron-doped diamond (BDD) electrode. J Hazard Mater 154:213–220. https://doi.org/10.1016/j.jhazmat.2007.10.011

Musielak M, Serda M, Gagor A et al (2024) Ultratrace determination and speciation of hexavalent chromium by EDXRF and TXRF using dispersive micro-solid phase extraction and tetraethylenepentamine graphene oxide. Spectrochim Acta, Part B 213:106863. https://doi.org/10.1016/j.sab.2024.106863

Nam S-N, Yea Y, Park S et al (2023) Modeling sulfamethoxazole removal by pump-less in-series forward osmosis–ultrafiltration hybrid processes using artificial neural network, adaptive neuro-fuzzy inference system, and support vector machine. Chem Eng J 474:145821. https://doi.org/10.1016/j.cej.2023.145821

Navalon S, Dhakshinamoorthy A, Alvaro M, Garcia H (2011) Heterogeneous Fenton catalysts based on activated carbon and related materials. Chemsuschem 4:1712–1730. https://doi.org/10.1002/cssc.201100216

Nourouzi MM, Chuah TG, Choong TSY, Rabiei F (2012) Modeling biodegradation and kinetics of glyphosate by artificial neural network. J Environ Sci Health B 47:455–465. https://doi.org/10.1080/03601234.2012.663603

Oliveira FH, Osugi ME, Paschoal FMM et al (2007) Electrochemical oxidation of an acid dye by active chlorine generated using Ti/Sn(1–x)Ir x O2 electrodes. J Appl Electrochem 37:583–592. https://doi.org/10.1007/s10800-006-9289-6

Ouarda Y, Trellu C, Lesage G et al (2020) Electro-oxidation of secondary effluents from various wastewater plants for the removal of acetaminophen and dissolved organic matter. Sci Total Environ 738:140352. https://doi.org/10.1016/j.scitotenv.2020.140352

Panizza M, Cerisola G (2003) Influence of anode material on the electrochemical oxidation of 2-naphthol. Electrochim Acta 48:3491–3497. https://doi.org/10.1016/S0013-4686(03)00468-7

Pavithra KG, Jaikumar V, Kumar PS, Sundarrajan P (2020) Cleaner strategies on the effective elimination of toxic chromium from wastewater using coupled electrochemical/biological systems. Environ Prog Sustain Energy 39. https://doi.org/10.1002/ep.13399

PubChem Hazardous Substances Data Bank (HSDB): 3430. https://pubchem.ncbi.nlm.nih.gov/source/hsdb/3430. Accessed 29 Aug 2023

Pulkka S, Martikainen M, Bhatnagar A, Sillanpää M (2014) Electrochemical methods for the removal of anionic contaminants from water – a review. Sep Purif Technol 132:252–271. https://doi.org/10.1016/j.seppur.2014.05.021

Qu X, Zheng J, Zhang Y (2007) Catalytic ozonation of phenolic wastewater with activated carbon fiber in a fluid bed reactor. J Colloid Interface Sci 309:429–434. https://doi.org/10.1016/j.jcis.2007.01.034

Rahemi V, Garrido JMPJ, Borges F et al (2013) Electrochemical determination of the herbicide bentazone using a carbon nanotube β-cyclodextrin modified electrode. Electroanalysis 25:2360–2366. https://doi.org/10.1002/elan.201300230

Rajasekaran N, Vinoba M, Al-Sheeha H, Rana MS (2021) The synergistic character of highly N-doped coconut–shell activated carbon for efficient CO_2 capture. ChemistrySelect 6:9149–9156. https://doi.org/10.1002/slct.202102522

Ricart M, Guasch H, Barceló D et al (2010) Primary and complex stressors in polluted mediterranean rivers: pesticide effects on biological communities. J Hydrol 383:52–61. https://doi.org/10.1016/j.jhydrol.2009.08.014

Rostami T, Jafarian M, Miandari S et al (2015) Synergistic effect of cobalt and copper on a nickel-based modified graphite electrode during methanol electro-oxidation in NaOH solution. Chin J Catal 36:1867–1874. https://doi.org/10.1016/S1872-2067(15)60959-7

Roy S, Dasgupta Ghosh B, Goh KL et al (2023) Pores on pores: a novel approach to fabricate super adsorbents from used face masks for large CO2 capture and dye removal. Carbon 206:422–433. https://doi.org/10.1016/j.carbon.2023.02.040

Saleh IA, Zouari N, Al-Ghouti MA (2020) Removal of pesticides from water and wastewater: chemical, physical and biological treatment approaches. Environ Technol Innov 19:101026. https://doi.org/10.1016/j.eti.2020.101026

Salman JM, Hameed BH (2010) Effect of preparation conditions of oil palm fronds activated carbon on adsorption of bentazon from aqueous solutions. J Hazard Mater 175:133–137. https://doi.org/10.1016/j.jhazmat.2009.09.139

Samaddoost L, Soltani M, Fatehifar E, Abbasi Asl E (2023) Design of amine-functionalized resin via a facial method with efficient CO2 capture from air. Process Saf Environ Prot 171:18–27. https://doi.org/10.1016/j.psep.2023.01.008

Sarkka H, Bhatnagar A, Sillanpaa M (2015) Recent developments of electro-oxidation in water treatment — a review. J Electroanal Chem 754:46–56. https://doi.org/10.1016/j.jelechem.2015.06.016

Spaltro A, Simonetti S, Laurella S et al (2019) Adsorption of bentazone and imazapyc from water by using functionalized silica: experimental and computational analysis. J Contam Hydrol 227:103542. https://doi.org/10.1016/j.jconhyd.2019.103542

Sridevi H, Bhat MR, Selvaraj R (2023) Removal of an agricultural herbicide (2,4-dichlorophenoxyacetic acid) using magnetic nanocomposite: a combined experimental and modeling studies. Environ Res 238:117124. https://doi.org/10.1016/j.envres.2023.117124

Sun Y, Li P, Zheng H et al (2017) Electrochemical treatment of chloramphenicol using Ti-Sn/γ-Al2O3 particle electrodes with a three-dimensional reactor. Chem Eng J 308:1233–1242. https://doi.org/10.1016/j.cej.2016.10.072

Sun W, Sun Y, Shah KJ et al (2019) Electrocatalytic oxidation of tetracycline by Bi-Sn-Sb/γ-Al2O3 three-dimensional particle electrode. J Hazard Mater 370:24–32. https://doi.org/10.1016/j.jhazmat.2018.09.085

Sun H, Li Y, Chen X et al (2023) Hypophosphorous acid functionalized nanoporous silicon for selective adsorption of Hg(II) in industrial waste water. Chem Eng Res Des 197:264–273. https://doi.org/10.1016/j.cherd.2023.07.024

Szpyrkowicz L, Kaul SN, Neti RN, Satyanarayan S (2005) Influence of anode material on electrochemical oxidation for the treatment of tannery wastewater. Water Res 39:1601–1613. https://doi.org/10.1016/j.watres.2005.01.016

Talaviya T, Shah D, Patel N et al (2020) Implementation of artificial intelligence in agriculture for optimisation of irrigation and application of pesticides and herbicides. Artificial Intelligence in Agriculture 4:58–73. https://doi.org/10.1016/j.aiia.2020.04.002

Tamai H, Shiraki K, Shiono T, Yasuda H (2006) Surface functionalization of mesoporous and microporous activated carbons by immobilization of diamine. J Colloid Interface Sci 295:299–302. https://doi.org/10.1016/j.jcis.2005.08.012

Tang N, Niu C-G, Li X-T et al (2018) Efficient removal of Cd2+ and Pb2+ from aqueous solution with amino- and thiol-functionalized activated carbon: isotherm and kinetics modeling. Sci Total Environ 635:1331–1344. https://doi.org/10.1016/j.scitotenv.2018.04.236

Tran ATK, Hyne RV, Pablo F et al (2007) Optimisation of the separation of herbicides by linear gradient high performance liquid chromatography utilising artificial neural networks. Talanta 71:1268–1275. https://doi.org/10.1016/j.talanta.2006.06.031

Üner O, Bayrak Y (2018) The effect of carbonization temperature, carbonization time and impregnation ratio on the properties of activated carbon produced from Arundo donax. Microporous Mesoporous Mater 268:225–234. https://doi.org/10.1016/j.micromeso.2018.04.037

Vasconcelos VM, Ponce-de-León C, Nava JL, Lanza MRV (2016) Electrochemical degradation of RB-5 dye by anodic oxidation, electro-Fenton and by combining anodic oxidation–electro-Fenton in a filter-press flow cell. J Electroanal Chem 765:179–187. https://doi.org/10.1016/j.jelechem.2015.07.040

Veljkovic A, Pohoryles DA, Bournas DA (2023) Heating energy demand estimation of the EU building stock: combining building physics and artificial neural networks. Energy and Buildings 298:113474. https://doi.org/10.1016/j.enbuild.2023.113474

Vlyssides A, Barampouti EM, Mai S et al (2004) Degradation of methylparathion in aqueous solution by electrochemical oxidation. Environ Sci Technol 38:6125–6131. https://doi.org/10.1021/es049726b

Wang C-T, Chou W-L, Kuo Y-M, Chang F-L (2009) Paired removal of color and COD from textile dyeing wastewater by simultaneous anodic and indirect cathodic oxidation. J Hazard Mater 169:16–22. https://doi.org/10.1016/j.jhazmat.2009.03.054

Wang Z, Qi J, Feng Y et al (2014) Preparation of catalytic particle electrodes from steel slag and its performance in a three-dimensional electrochemical oxidation system. J Ind Eng Chem 20:3672–3677. https://doi.org/10.1016/j.jiec.2013.12.065

Wang X, Guo Q, Kong T (2015) Tetraethylenepentamine-modified MCM-41/silica gel with hierarchical mesoporous structure for CO2 capture. Chem Eng J 273:472–480. https://doi.org/10.1016/j.cej.2015.03.098

Wang C, Chen L, Liu S (2019) Activated carbon fiber for adsorption/electrodeposition of Cu (II) and the recovery of Cu (0) by controlling the applied voltage during membrane capacitive deionization. J Colloid Interface Sci 548:160–169. https://doi.org/10.1016/j.jcis.2019.04.030

Wang T, Song Y, Ding H et al (2020) Insight into synergies between ozone and in-situ regenerated granular activated carbon particle electrodes in a three-dimensional electrochemical reactor for highly efficient nitrobenzene degradation. Chem Eng J 394:124852. https://doi.org/10.1016/j.cej.2020.124852

Wang Y, Cui C, Zhang G et al (2021) Electrocatalytic hydrodechlorination of pentachlorophenol on Pd-supported magnetic biochar particle electrodes. Sep Purif Technol 258:118017. https://doi.org/10.1016/j.seppur.2020.118017

Wang J, Liu Y, Zhu B et al (2024) Ultrasonic-assisted preparation of organic amine-modified SBA-15 for CO2 capture in wide temperature range: experimental and computational investigation. J Energy Inst 113:101555. https://doi.org/10.1016/j.joei.2024.101555

Wu Z, Cong Y, Zhou M, Tan T (2005) p-Nitrophenol abatement by the combination of electrocatalysis and activated carbon. Chem Eng J 106:83–90. https://doi.org/10.1016/j.cej.2004.10.009

Wu W, Huang Z-H, Lim T-T (2016) A comparative study on electrochemical oxidation of bisphenol A by boron-doped diamond anode and modified SnO2-Sb anodes: influencing parameters and reaction pathways. J Environ Chem Eng 4:2807–2815. https://doi.org/10.1016/j.jece.2016.05.034

Wu Z, Liu Y, Wang S et al (2019) A novel integrated system of three-dimensional electrochemical reactors (3DERs) and three-dimensional biofilm electrode reactors (3DBERs) for coking wastewater treatment. Biores Technol 284:222–230. https://doi.org/10.1016/j.biortech.2019.03.123

Wu X, Song X, Chen H, Yu J (2021) Treatment of phenolic compound wastewater using CuFe2O4/Al2O3 particle electrodes in a three-dimensional electrochemical oxidation system. Environ Technol 42:4393–4404. https://doi.org/10.1080/09593330.2020.1760356

Xiao M, Zhang Y (2016) Electro-catalytic oxidation of phenacetin with a three-dimensional reactor: degradation pathway and removal mechanism. Chemosphere 152:17–22. https://doi.org/10.1016/j.chemosphere.2015.12.026

Xiao H, Hao Y, Wu J et al (2023) Differentiating the reaction mechanism of three-dimensionally electrocatalytic system packed with different particle electrodes: Electro-oxidation versus electro-Fenton. Chemosphere 325:138423. https://doi.org/10.1016/j.chemosphere.2023.138423

Yang Y, Liu Y, Liu S et al (2024) Experimental and theoretical investigation of amine-modified biomass-derived activated carbon for CO2 capture: the effects of carbon chain length and types of amine. Chem Eng Sci 292:119968. https://doi.org/10.1016/j.ces.2024.119968

Yu D, Cui J, Li X et al (2020) Electrochemical treatment of organic pollutants in landfill leachate using a three-dimensional electrode system. Chemosphere 243:125438. https://doi.org/10.1016/j.chemosphere.2019.125438

Zhang T, Liu Y, Yang L et al (2020) Ti–Sn–Ce/bamboo biochar particle electrodes for enhanced electrocatalytic treatment of coking wastewater in a three-dimensional electrochemical reaction system. J Clean Prod 258:120273. https://doi.org/10.1016/j.jclepro.2020.120273

Zhang J, Zuo J, Ai W et al (2021) Preparation of mesoporous coal-gasification fine slag adsorbent via amine modification and applications in CO2 capture. Appl Surf Sci 537:147938. https://doi.org/10.1016/j.apsusc.2020.147938

Zhang J, Xu W, Ma J, Jia Q (2023) Design of reversibly charge-changeable rhodamine B modified magnetic nanoparticles to enrich phosphopeptides. J Chromatogr A 1697:463992. https://doi.org/10.1016/j.chroma.2023.463992

Zhao X, Ding Y, Ma L et al (2023) An amine-functionalized strategy to enhance the CO2 absorption of type III porous liquids. Energy 279:127975. https://doi.org/10.1016/j.energy.2023.127975

Zheng T, Wang Q, Shi Z et al (2016) Advanced treatment of wet-spun acrylic fiber manufacturing wastewater using three-dimensional electrochemical oxidation. J Environ Sci 50:21–31. https://doi.org/10.1016/j.jes.2016.03.020

Zhou M, Lei L (2006) The role of activated carbon on the removal of p-nitrophenol in an integrated three-phase electrochemical reactor. Chemosphere 65:1197–1203. https://doi.org/10.1016/j.chemosphere.2006.03.054

Zhu Y, Zhao C, Liang J et al (2019) Rapid removal of diclofenac in aqueous solution by soluble Mn(III) (aq) generated in a novel Electro-activated carbon fiber-permanganate (E-ACF-PM) process. Water Res 165:114975. https://doi.org/10.1016/j.watres.2019.114975

Publisher's Note Springer Nature remains neutral with regard to jurisdictional claims in published maps and institutional affiliations.

Springer Nature or its licensor (e.g. a society or other partner) holds exclusive rights to this article under a publishing agreement with the author(s) or other rightsholder(s); author self-archiving of the accepted manuscript version of this article is solely governed by the terms of such publishing agreement and applicable law.